

Photodynamic performance of amphiphilic chlorin e6 derivatives with appropriate properties: A comparison between different-type liposomes as delivery systems

Agnieszka Szurko^a, Marzena Rams-Baron^a, Franz-Peter Montforts^b, Daniela Bauer^b, Patrycja Kozub^a, Jerzy Gubernator^c, Sandra Altmann^a, Agata Stanek^{d,*}, Aleksander Sieron^{e,f}, Alicja Ratuszna^a

^a Faculty of Science and Technology, University of Silesia, 75. Pułku Piechoty 1A, 41-500, Chorzów, Poland

^b Institute of Organic Chemistry, University of Bremen, Leobener Strasse NW2C, D-28359, Bremen, Germany

^c Faculty of Biotechnology, University of Wrocław, Fryderyka Joliot-Curie 14a, 50-383, Wrocław, Poland

^d Faculty of Medical Sciences in Zabrze, Medical University of Silesia, Department of Internal Medicine, Angiology and Physical Medicine, Batorego 15, 41-902, Bytom, Poland

^e Department of Internal Medicine, Angiology and Physical Medicine, No. 2 Specialist Hospital, Batorego 15, 41-902, Bytom, Poland

^f Jan Długosz University in Częstochowa, Jerzego Waszyngtona 4/8, 42-200 Częstochowa, Poland

ARTICLE INFO

Keyword:

Amphiphilic chlorin e6 derivatives
Photodynamic therapy
Human colon Adenocarcinoma cells (HCT116 and HCT116 p53-/-)
Liposomes

ABSTRACT

Background: Many aspects are currently being investigated, with the aim of improving the application of PDT in the clinic by rendering it more effective. One of the current trends focuses on the use of nanocarriers. The aim of this study is to describe novel photosensitizers among polyol amide chlorin e6 derivatives for photodynamic therapy (PDT) using liposomes.

Methods: In addition to their intracellular localization and antiproliferative activity against HCT116 cells, appropriate photophysical features have been determined (especially high $^1\text{O}_2$ quantum yield production).

Results and conclusions: Fluorescent microscopy demonstrated that the compounds entered the endoplasmic reticulum (ER), lysosomes, mitochondria and partially the cytoplasm. All of the chlorins showed no dark cytotoxicity; however, high phototoxicity was observed. Using optical and electron microscopy, we investigated the impact of chlorin-based PDT upon cell damage leading to cell death. Chl ara 3 was identified as the most promising compound among polyol amide chlorin e6 derivatives and improved phototoxicity was observed as compared with a clinically approved temoporfin. Our results indicate that newly-synthesized chlorins seem to be promising candidates for PDT application, and two of them (chl ara 3 and chl mme 2) may create promising new drugs, both in the form of a free compound and as a liposomal formulation.

1. Introduction

Photodynamic therapy is a non-invasive treatment based on the administration of photosensitizers (PS) and non-ionizing light. These elements, in the presence of oxygen, are sufficient to induce photochemical reactions that destroy malignant tissue without major side effects [1]. Since the efficacy of PDT is largely dependent on the properties of PS, these compounds should be characterised by: (1) high accumulation at the tumour tissue (preferably amphiphilicity, which improves drug accumulation), (2) low dark toxicity, (3) high absorption coefficients in the spectrum region of 600–800 nm, (4) high phototoxicity conditioned by the efficient generation of peroxides and free

radicals (type I reaction) and/or reactive cell-damaging singlet oxygen ($^1\text{O}_2$) (type II reaction), (5) chemical stability both in darkness and during irradiation, (6) chemical purity and accessibility [2,3]. Additionally, photosensitizers should have a moderate fluorescence quantum yield (Φ_f), favourable to photodynamic diagnosis (PDD). Excessive Φ_f may reduce the therapeutic efficiency of PDT by limiting Φ_T production ($\Phi_f + \Phi_T \leq 1$) [4]. Effective penetration of PS into the site of its activity is equally important, as the $^1\text{O}_2$ diffusion path ranges from only 10 nm–55 nm [5]. Thus, the sites of induced photodamage reveal the subcellular location of photosensitizer [6].

The most commonly used PS are porphyrin derivatives, chlorins, bacteriochlorins, phthalocyanines, naphthalocyanines or taxaphyrins.

* Corresponding author at: Department of Internal Medicine, Angiology and Physical Medicine, Batorego Street 15, 41-902, Bytom, Poland.

E-mail addresses: agnieszka.szurko@us.edu.pl (A. Szurko), astanek@tlen.pl (A. Stanek).

<https://doi.org/10.1016/j.pdpdt.2020.101799>

Received 9 February 2020; Received in revised form 11 April 2020; Accepted 24 April 2020

Available online 05 May 2020

1572-1000/ © 2020 Elsevier B.V. All rights reserved.

Although the best-studied group of photosensitizers are porphyrin derivatives, unfortunately all of them tend to aggregate, which affects their limited cytotoxic properties. It has been shown that the ability to produce free radicals decreases along with increasing aggregation [7,8]. Chlorins and bacteriochlorins are reduced porphyrins with one and two reduced double bonds in pyrrole rings, respectively. These photosensitizers can be obtained both by chemical synthesis and by the modification of molecules of natural origin, such as protohexine or chlorophyll *a* [9]. They have strong absorption maxima; for chlorins at about 650 nm and for bacteriochlorins at 710 nm [10,11]. The last Q band in absorption spectra is much more intense and shifted towards longer wavelengths, which makes them more useful in photodynamic therapy. Chlorins are also more stable in solutions than bacteriochlorins [12]. A significant problem affecting porphyrins and aromatic systems, in general, is aggregation [4]. Hydrophobic porphyrins form dimers or higher aggregates much easier, but on the other hand, their hydrophobicity determines easy penetration through cell membranes [13]. Amphiphilic chlorins still have a high affinity for cell membranes but a lower tendency to aggregate, since amphiphilicity regulates this phenomenon and thus affects the photophysical properties of the compound [7].

Chlorins, however, do not show such great solubility problems as in the case of phthalocyanines and naphthalocyanines, which are strongly hydrophobic compounds and consequently do not dissolve in most injection fluids, which significantly limits their use. In addition, the amphiphilic character of the investigated chlorin derivatives allows good penetration through phospholipid membranes in the cell.

One of the chlorins which has attracted widespread attention thanks to its advantageous photophysical properties and numerous successful modifications, e.g. nanoparticles, [14] nanomicelles [15], and nanovectors [16], is chlorin e6. Also, conjugations of this PS with peptides, lipoproteins, sugars, polyethylene glycols, and polyamines to increase the PDT efficiency, have been reported [17–22]. Several glycoconjugates of chlorins [23], porphyrins [24–26] and phthalocyanines [27] have recently been developed since glycoconjugation allows for effective binding to sugar-binding lectin-type receptors in some types of malignant cells [24,28]. This paper describes the results obtained for three novel chlorin e6 derivatives. Two of them were covalently linked with polyol amines derived from glucose and arabinose. The novel polyolamide chlorin e6 derivatives show striking beneficial differences compared with the known porphyrinoid sensitizers with attached hydrophilic moieties such as carbohydrates, including: (1) a non-ionic neutral hydrophilic character, avoiding severe electrostatic interactions, (2) stereochemical homogeneousness due to the missing anomeric centres of the ‘carbohydrate’ moieties, (3) presence of rigid amide linkages between the chlorin and ‘carbohydrate’ units, avoiding division into the subunits, (4) effective preparation due to the simple and preferred formation of the amide linkages. The tested photosensitizers were also designed for their potential application in the form of liposome carriers. As it is known, liposomes create great opportunities to solve one of the main challenges of photodynamic therapy, which is effective drug delivery to cells.

More recently, we have also shown that the co-application of the redox-active chelators (TSCs) and one of the chlorins (chl ara 3) presented here can exert a better total therapeutic effect than the sum of the effects caused by each compound separately (synergistic effect) [29]. The use of combination therapy offers great hope for the creation of a personalized therapeutic approach to the patient. Often, combined therapy not only increases the therapeutic effect while reducing drug doses but also simultaneously impacts various molecular targets. That is why it is so important to examine in detail the physicochemical properties, kinetics of compound retention in cells, the intracellular localization and the anti-tumour activity of our e6 chlorin derivatives.

2. Materials and methods

2.1. General

Starting materials and reagents were either prepared according to literature procedures or were purchased from Fluka, Merck or Aldrich and used without further purification. All solvents were purified and dried by standard methods. All chemical reactions were carried out under argon. ^1H NMR and ^{13}C spectra were measured with Bruker DPX-200 Avance or Avance NB-360 MHz spectrometers; all chemical shifts were referenced to the tetramethylsilane lock signal. MS and HRMS were performed on a Finnigan MAT 8200 spectrometer (EI (70 eV), DCI (NH_3 , 8 mA s^{-1}) and ESI (solvent)) while ESI-HRMS was performed with an APEX Qe9.4 T instrument (9.4 T superconducting magnet) with an Apollo II electrospray ioniser. IR spectra were measured with a Perkin-Elmer Paragon 500 FTIR spectrometer. UV/VIS analysis was carried out on a Varian Cary 50 spectrophotometer. Melting points are uncorrected and were determined on a Reichert Thermovar hot-stage apparatus.

2.2. Spectroscopic measurements

The ground-state absorption and fluorescence spectra were recorded at room temperature using a U-2900 spectrofluorometer and F-7000 spectrophotometer (Hitachi) with DMSO as the solvent. Fluorescence quantum yields were determined in ethanol using a comparative method with TPP (Sigma) in toluene as standard ($\Phi_f = 0.11$ [30]). Transient triplet-triplet absorption spectra were measured using an LKS 60 laser flash photolysis spectrometer (Applied Photophysics). To excite the samples, the third harmonic (355 nm) of Nd:YAG laser (20 Hz Brilliant, Quantel) was used. All solutions were prepared in ethanol with an equal absorbance (*A*) value at the excitation wavelength ($A_{355} = 0.2$). The quantum yields of singlet oxygen generation were defined using the comparative method, which is based on the detection of $^1\text{O}_2$ phosphorescence (at around 1270 nm). Samples and the reference solution were prepared in ethanol and optically matched at the excitation wavelength 355 nm ($A_{355} = 0.25$). Measurements were taken with phenalene (Sigma) in ethanol as standard ($\Phi_A = 0.95$ [31]).

2.3. Photostability studies

The photostability of chlorin derivatives was verified using a Hitachi U-2900 spectrophotometer. The absorption spectra were recorded before and after red light irradiation (halogen lamp, 630 nm longpass filter). The solutions were illuminated for various periods of time with different light doses ranging from 4.56 to 20.52 J/cm². Three independent experiments were performed, all at a distance of 1 cm from the light source. The fluence rate of the halogen lamp ($\lambda \geq 630$ nm) was 380 W/m². During exposure, solutions were kept at room temperature and magnetically stirred. Our lighting system is not standard in medical applications, which is a drawback. However, there are studies that allow the calculation of the actual dose of light, taking into account the correction of the dose by the number of absorbed photons, which gives the opportunity to correctly assess the PDT effect for all light sources [32].

2.4. Liposome preparation

MLVs were prepared by the hydration of the dry lipid film. Solutions of phospholipids and cholesterol were prepared at a concentration of 10 mg/mL in a mixture of chloroform and methanol at a ratio of 1:1. Table 1 shows the exact composition of liposomes and molar relations between individual components. Compounds (chl mme 2 and chl ara 3) were dissolved in a mixture of chloroform and ethanol at a ratio of 1:1. The appropriate amounts of lipids and chlorins in organic solvents were mixed, and solvents were evaporated using a vacuum evaporator to

Table 1
Lipid composition of individual liposomes used for research.

Composition of liposomes	Mole ratio	The type of liposomes with regard to the charge on the surface of the phospholipid membrane
HSPC/Chol	7:3	Neutral
HSPC/DSPE-PEG ₂₀₀₀	9.5:0.5	Neutral
HSPC/DOTAP/Chol	6:1:3	Cationic
HSPC/DOTAP/DSPE-PEG ₂₀₀₀	8.5:1:0.5	Cationic
DPPC/DPPG	9:1	Anionic
HSPC/DSPG/DSPE-PEG ₂₀₀₀	8.5:1:0.5	Anionic

HSPC – L- α -phosphatidylcholine, hydrogenated (Soy); Chol – cholesterol; DSPE-PEG₂₀₀₀ – distearoylphosphatidylethanolamine-poly(ethylene glycol); DOTAP – 1,2-dioleoyl-3-trimethylammonium-propane; DPPC – 1,2-dipalmitoylphosphatidylcholine; DPPG – 1,2-dipalmitoylphosphatidylglycerol; DSPG – distearoylphosphatidylglycerol.

obtain a dry lipid film distributed evenly on the walls of the flask. Then, to dry the lipid film, the flasks were placed in a freeze dryer for one hour. The lipid film was rehydrated with PBS by vortexing at a temperature of 64 °C above the lipid phase transition temperature. Using a pressure calibrator (LIPOKAL pressure calibrator from P.P.H. Marker) with compressed nitrogen, liposomes were passed through polycarbonate membrane filters with a pore diameter of 100 nm (Nucleopore, Whatman) eight times. As a result, unilamellar liposomes containing 100 μ M concentration of the tested chlorins encapsulated in a phospholipid bilayer were obtained.

2.5. Size and polydispersity index (PDI) of differently charged liposomes

The particle size analyzer Zetasizer Nano ZS (Malvern) was used to measure the diameter and the polydispersity index (PDI) of the obtained liposomes by dynamic light scattering (DLS). The light source was an He-Ne laser (red, 633 nm), whose detection angle is 173° and the measuring range varies from 0.6 nm to 6 μ m. Liposomes were diluted 100-fold with PBS at a pH 7.4. The experiment was conducted in polystyrene cuvettes with an optical path of 1 cm at room temperature.

2.6. Stability of liposomes

The stability experiments consisted of measuring the diameter and determining the PDI index of liposomes in the days following their preparation. The liposome suspension was stored under limited light at 3 °C. Measurements were carried out in the same way as in point 2.5 (size).

2.7. Encapsulation efficiency of chlorins into liposomes (EE%)

The encapsulation efficiency of photosensitizers into liposomes was determined using spectrophotometric and Steward methods for the chlorin and phospholipids concentration measurements, respectively. The Steward method uses the ability to form a chloroform-soluble complex of phospholipid and iron(III) thiocyanate. Non-encapsulated photosensitizers were removed from the chlorin-containing liposomes by size exclusion chromatography on a Sephadex G-50 Fine gel mini-columns (5.5 mm x 70 mm) equilibrated with phosphate buffer [33]. The 50 μ L of liposome suspension was applied to the column to remove the nonencapsulated PS. A sample of liposomes for spectrophotometric measurements was prepared in 1 mL of ethanol to dissolve the phospholipid bilayer and release the photosensitizer. The Hitachi F-7000 and Hitachi U-2900 spectrophotometers were used to determine the compound and phospholipid concentration, respectively. The measurements were carried out at room temperature and in both cases, using a quartz cuvette with an optical path of 1 cm. Three independent

experiments were performed for each type of liposome. Using Formula 1 below, the percentage encapsulation efficiency of photosensitizers in liposomes was calculated [34].

Formula 1

$$\%EE = \frac{\text{Drug} \left[\frac{\text{mg}}{\text{mL}} \right]}{\text{Lipid} \left[\frac{\text{mg}}{\text{mL}} \right]} \cdot \frac{\text{Initial } \frac{D}{L}}{L} \cdot 100\%$$

%EE – The percentage of drug encapsulation efficiency;

Drug – concentration of tested photosensitizer;

Lipid – phospholipid concentration;

Initial D/L – initial value of the drug / phospholipid ratio determined at the time of hydration of the thin phospholipid film.

2.8. Cancer cell lines and culture conditions

The biological *in vitro* studies were carried out with HCT116 cells. Cytotoxicity and phototoxicity studies were also performed using cells with the p53 gene knockout (HCT116 p53^{-/-}). The cells were grown in a Dulbecco's Modified Eagle's Medium (DMEM, Sigma), supplemented with 12 % fetal bovine serum (FBS, Gibco) and antibiotics (Gentamycin, Polfa) under standard conditions (humidified atmosphere with 5% CO₂ at 37 °C).

All used cell lines, the human colorectal carcinoma cell line (HCT116) and its variant with knock-out of p53 gene (HCT116p53^{-/-}), came from the collection obtained from the Center for Translation and Molecular Biology of Cancers of the Institute of Oncology in Gliwice. The HCT116p53^{-/-} cell line, whose authors are K. W. Kinzler and B. Vogelstein, was brought from the USA to the Institute of Oncology in 2001 [35].

2.9. Cytotoxicity and phototoxicity

Cells were seeded at a density of 3 × 10⁵ cells/35 mm Petri dish (Nunc). After 18 h, the culture medium was replaced with a medium containing different chlorin concentrations (the final DMSO concentration ≤ 0.3 %). After 3.5 h of incubation, the cells were rinsed with phosphate buffered-saline (PBS, pH 7.2). The dishes intended for dark toxicity measurements were then supplemented with 1 mL of culture medium and after 24 h cell viability was assessed using the MTS assay. Concurrently, 1 mL of DMEM without phenol red was added to cells designed for phototoxicity measurements and subsequently they were irradiated with a halogen lamp (630 nm longpass filter; 20 J/cm²; all experiments were performed at a distance of 1 cm from the light source). Cell viability was measured using the MTS assay (24 h post irradiation) or clonogenic assay (immediately after irradiation) as described elsewhere [36]. During each experiment, non-treated cells (no light, no photosensitizer) and cells exposed only to the light (no incubation with photosensitizer) were used as controls. Photodynamic efficiency was compared to temoporfin activity (Biolitec Pharma Ltd.).

2.10. Statistical analysis

The analysis of cell viability was performed using GraphPad Prism v.5.0 software (GraphPad Software, USA). MTS assays were repeated a minimum of three times independently. Each experiment included six replicated data points. The normality of variable distribution was assessed using the Shapiro-Wilk test. In order to detect significant differences between mean values, the non-parametric Mann-Whitney U test was used.

2.11. The kinetics of photosensitizers uptake

To determine the kinetics of the cellular uptake of the photosensitizers, spectrophotometric measurements of cell lysates were taken

treated control cells. Additionally, three-dimensional graphs of excitation vs. emission were recorded.

2.12. Intracellular localization (fluorescence microscopy)

To investigate the photosensitizer subcellular localization, fluorescence microscopy was applied. The cells were seeded (2×10^4 cells/well) in 8-well chambered cover glasses (Nunc). After 18 h, the culture medium was replaced with a medium containing photosensitizer (2.5 μM) for an additional 2 h. The cells were then rinsed twice with PBS (pH 7.2) and a pre-warmed (37 °C) organelle specific dye-containing medium was added. Prior to microscope observation, the cells were washed again (3 x PBS) and placed in a fresh medium without phenol red. Image analysis was carried out using the system designed for long-duration cell bioluminescence imaging, composed of an inverted fluorescence microscope (Model IX81, Olympus) equipped with a CO₂ incubator (temperature, humidity and gas flow under control).

2.13. Cryo scanning electron microscopy (Cryo-SEM)

HCT116 cells were seeded (6×10^4 cells/well) onto coverslips (Thermanox® Plastic Coverslips, Nunc™), which were kept in 24-well plates and cultured for 18 h under standard conditions. PDT was carried out as described previously (section 4.6, chlorin concentration 2.5 μM). Microscopic analysis was performed 24 h post irradiation. The cells were then fixed and dehydrated in a series of increasing ethanol concentrations. Before observation, the coverslips were mounted onto the specimen holder and dipped into liquid nitrogen. After ice sublimation, the coverslips were coated with approximately 5 nm of platinum, and the samples were transferred into the (microscopic) analysis chamber. The observation was performed using a Joel 7600 F scanning electron microscope at a temperature of -130 °C with 2–15 kV accelerating voltage.

2.14. Toxicity of liposomes

The MTS test was performed to determine the toxicity of chlorins encapsulated in liposome carriers on HCT116 cells. The medium of cells previously sown in Petri dishes was changed to Opti-MEM® I and the following volumes of empty liposomes and liposomes with the photosensitizer tested were administered: 5 μl , 10 μl , 25 μl , 50 μl . Thus, the following concentrations of tested chlorins were obtained: 0.5 μM , 1 μM , 2.5 μM and 5 μM , respectively. After 4 h of incubation, the cells were rinsed with phosphate buffer, and the medium was again changed for a standard one. The MTS was performed after the subsequent 24 h. The experiments were performed in the dark.

2.15. Liposome carriers in chlorin-PDT therapy

The phototoxicity of chlorins administered in liposomes was also determined by the standard MTS test. Compounds were administered

analogously to the dark toxicity study. After the incubation of the cells with chlorin-containing liposomes, they were irradiated. The light source was a collimated LED beam with a wavelength of 660 nm (M660 L3-C4, Thorlabs). The 4.2 and 12.5 J/cm² light doses were used. After irradiation, the medium was also replaced, and the plates were incubated for the subsequent 24 h, as cells for the dark toxicity test. After 24 h, the cell viability relative to that obtained by cell treatment with free photosensitizer was assessed with the MTS test. Free chlorin solutions were diluted first in a small amount of DMSO and in culture medium to obtain concentrations appropriate to those used in liposome formulations. The experiments were carried out under sterile conditions limiting the influence of external light. Statistical analysis was performed on the results obtained from at least three independent experiments. First, the normality of distribution was checked using the Shapiro-Wilk test. Then, using the nonparametric Mann-Whitney *U* test to compare two independent groups, statistical analysis was performed. The differences between the analysed variables were considered statistically significant when the *p* value < 0.05. Control cells (not treated with either photosensitizer or light) were taken as 100 %.

3. Results

3.1. Synthesis of chlorin derivatives

Chlorins 2, 3 and 4 were originally derived from chlorin e6 trimethylester (chl tme 1) (Scheme 1). Chl tme 1 can be obtained from cyanobacteria using the isolation and modification process [37–39]. The advantage of cyanobacteria is that the bacteria produce only chlorophyll *a*, whereas plants contain a mixture of chlorophyll *a* and *b*. Selective hydrolysis of chl tme 1 yields chlorin e6 13-monomethylester (chl mme 2) as a crystalline compound of high purity [38–40]. The free carboxylic acid functions of chl mme 2 were activated with *iso*-butyl chloroformate and then reacted with *L*-1-amino-1-deoxy-arabitol [38] or commercially available glucamine to yield chlorin e6 bis-arabitylamide (chl ara 3) and chlorin e6 bis-glucamide (chl glc 4), respectively [38,39]. Due to their amphiphilic character, compounds 3 and 4 were purified by reversed phase chromatography (silicagel RP-18, MeOH / H₂O, 1 + 1). The purity (in all cases > 95 %) of synthesized compounds 2, 3 and 4 was confirmed by chromatography and various spectroscopic methods (¹H-NMR, MS, HRMS IR, UV/Vis). The detailed synthesis was described in the publication by Bauer et al. [38,39].

3.2. Absorption and fluorescence

From the point of view of PS application in photodynamic therapy, the most important are the properties of the last Q band. It should be shifted as much as possible in the direction of longer wavelengths, and it has the highest possible value of the molar absorption coefficient. The absorption spectra of PS include an intense Soret band at about 400 nm and broad bands in the visible region called the Q bands. In the case of all chlorins, the position of the most red-shifted Q band is similar (ca.

Table 2
Absorption and fluorescence properties of chlorin e6 derivatives 2 - 4.

Compound	Absorption ^a λ / nm (ϵ / M ⁻¹ cm ⁻¹)						Fluorescence		E_s / kJ mol ⁻¹
	λ_{max} ^a / nm	ϵ	λ_{max}	ϵ	λ_{max}	ϵ	λ_{max} ^a / nm	Φ_f ^b	
chl ara 3	406.5 (8.72 · 10 ⁴)	503 (8.23 · 10 ³)	533 (4.77 · 10 ³)	560.5 (3.06 · 10 ³)	609 (4.02 · 10 ³)	666 (2.31 · 10 ⁴)	674	0.25	182
chl glc 4	408 (2.91 · 10 ⁴)	503 (2.75 · 10 ³)	535 (1.61 · 10 ³)	561 (1.39 · 10 ³)	607 (1.31 · 10 ³)	665.5 (6.78 · 10 ³)	674	0.24	182
chl mme 2	403 (1.13 · 10 ⁵)	501 (1.02 · 10 ⁴)	530 (4.17 · 10 ³)	560 (2.16 · 10 ³)	608 (4.09 · 10 ³)	663.5 (2.69 · 10 ⁴)	673	0.27	183

^a in DMSO.

^b in ethanol.

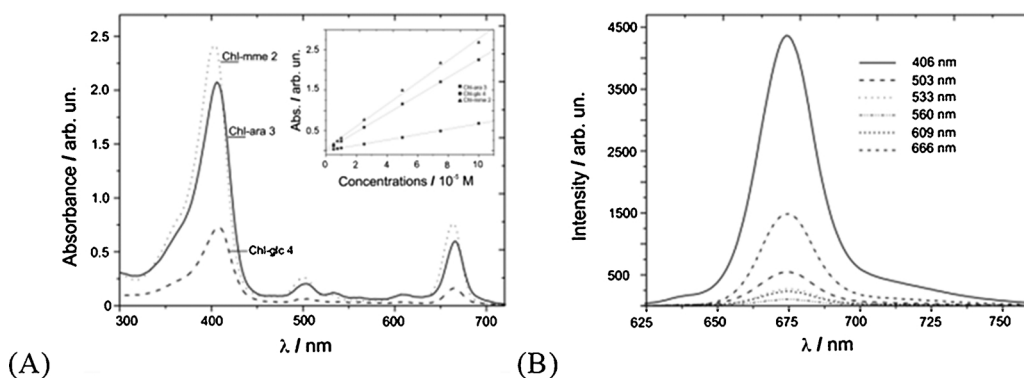


Fig. 1. Ground-state absorption spectra of chlorin solutions in DMSO (5 μM) (A). Insert shows the relation between the last Q band absorbance values and sample concentrations. Deviations from the Lambert-Beer's law, which indicate aggregation, were not observed. (B) The graph shows the fluorescence spectra of chl ara 3 in the DMSO solution (5 μM) after excitation with different wavelengths.

665 nm), but the corresponding value of the molar absorption coefficient is the highest for chl mme 2 ($\epsilon > 10^4 \text{ mol}^{-1} \text{ cm}^{-1}$) (Table 2). In the analysis of solutions aggregation, the obtained relation $A = f(c)$ was linear, suggesting that it did not occur. The fluorescence spectra (Fig. 1) exhibit a strong emission band with a maximum of 674 nm, depending on the chlorin. From the intersection of the normalized absorption and fluorescence spectra, the singlet state energies were estimated to be 182 kJ mol^{-1} and 183 kJ mol^{-1} . Additionally, the Stokes shift was calculated as the difference (in wavelength unit) between the positions of the maximum emission and the last absorption band maximum. Calculated values were 8 nm – 9.9 nm, depending on the compound. Furthermore, the excitation and absorption spectra were in excellent tally, thus indicating the chemical purity of the examined samples. Fluorescence quantum yields were determined in ethanol using a comparative method with tetraphenylporphyrin (TPP) as standard ($\Phi_f = 0.11$ [30]). The compounds have a moderately high value of fluorescence quantum yields (0.24–0.27), which may be useful in their application in photodynamic diagnostics. High values of molar absorption coefficients of the tested compounds pre-qualified them for use in PDT.

3.3. Triplet state lifetimes

The triplet-triplet absorption spectra of the chlorins show features such as an intense absorption band of 450 nm and ground state bleaching bands (see example in Figure S1). The measured decay curves that occur after the laser excitation show the process of reducing the population of the photosensitizer molecules in the triplet state and can be described as the kinetic equation for the first order reaction. The triplet state lifetime was calculated (Table 3) as the reverse rate constant characterizing this process. Efficient generation of $^1\text{O}_2$ is obtainable due to the following properties of PS triplet state: long lifetime (in a microseconds range) and energy sufficient for $^1\text{O}_2$ formation ($\geq 94 \text{ kJ mol}^{-1}$) [2,41].

The obtained triplet state lifetimes were in the range of 0.23–0.27 μs . This range was comparable to the value designated by Zenkevich for chlorin e6, which in the presence of oxygen was 0.29 μs [42]. Additionally, the result for TPP is presented. The calculated triplet lifetime value of 0.36 μs corresponds to the result obtained by Silva et al. [43]. Furthermore, it was observed that the triplet state lifetimes of

Table 3
Triplet state lifetimes and singlet oxygen quantum yields of chlorin e6 derivatives 2 – 4 in ethanol measured by laser flash photolysis.

Compound	Triplet lifetime / μs	$^1\text{O}_2$ quantum yield
Phenalenone	–	0.95 ³⁸
TPP	0.36 \pm 0.01	0.66
chl ara 3	0.27 \pm 0.02	0.63
chl glc 4	0.24 \pm 0.01	0.56
chl mme 2	0.23 \pm 0.01	0.66

deoxygenated samples (argon bubbling) grow, which confirms that oxygen functioned as an active quencher in the process.

3.4. Singlet oxygen

The $^1\text{O}_2$ phosphorescence spectrum with the maximum of 1271 nm is shown in Fig. 2D. The singlet oxygen quantum yields ($\Phi\Delta$) were calculated as described elsewhere [44] (Table 3). The measured values of $\Phi\Delta$ correspond to the following relation: chl mme 2 > chl ara 3 > chl glc 4. The results are comparable to the literature value of the singlet oxygen quantum yield for chlorin e6, which is 0.65 in ethanol [42,45]. In addition, in order to validate the method applied, we measured the singlet oxygen quantum yield of TPP in toluene (in reference to phenalenone $\Phi\Delta = 0.95$ [31]). The obtained singlet oxygen quantum yield of 0.66 agreed with the value reported by Redmond ($\Phi\Delta = 0.68$ [45]). The average lifetime of singlet oxygen obtained in toluene was 30.6 μs , which is comparable with the values found in the literature [46].

3.5. The stability and photodegradation

The processes related to the photosensitizer instability or photodegradation influence both the effectiveness of the therapy and the safety for the patient. In PDT, some degradation can be good if it improves the way the body releases the sensitizing factor after the therapeutic procedure. The photodegradation process also has its disadvantages with regard to optimal light dosimetry and the choice of drug concentration [47]. Moreover, photobleaching is more complex in *in vitro* conditions. Even medium supplementation with 1% fetal calf serum (FCS) increased the degree of photobleaching [9]. Therefore, in order to reduce the risk of the serum impact, our PDT *in vitro* experiments (cell irradiation after chlorin incubation) were performed in medium without fetal bovine serum (FBS) and phenol red.

We analysed many aspects important for determining the properties of chlorin derivatives. Preliminary photodegradation studies mainly aimed to check whether the compounds did not undergo photobleaching during irradiation and whether the therapeutic effect could be obtained. Nevertheless, the potential photosensitizer should be stable both in the dark and during exposure. Firstly, we estimated the chemical stability of the chlorins in darkness. After one week, only a small change in the band intensity was observed (see Figure S2).

As is known from the literature, photobleaching processes of mono-L-aspartylchlorin e6 (in PBS pH 7.4; irradiated at 400 nm) follow a first-order kinetic until 70 % of the sensitizer is bleached [48]. The photobleaching may occur at different rates depending on the solvent as observed for this chlorin (faster in fetal calf serum FCS than in PBS; irradiated at 405 nm – 415 nm) [49]. To determine the photostability of photosensitizers, we collected the absorption spectra following irradiation with different red-light doses (4.56–22.80 J/cm^2) and assessed the ratio of absorbance for the most red-shifted Q band measured after and before exposure (S6-S8). The fluence rate of the halogen lamp ($\lambda \geq 630 \text{ nm}$) was 380 W/m^2 when measured from a distance of 1 cm. At the

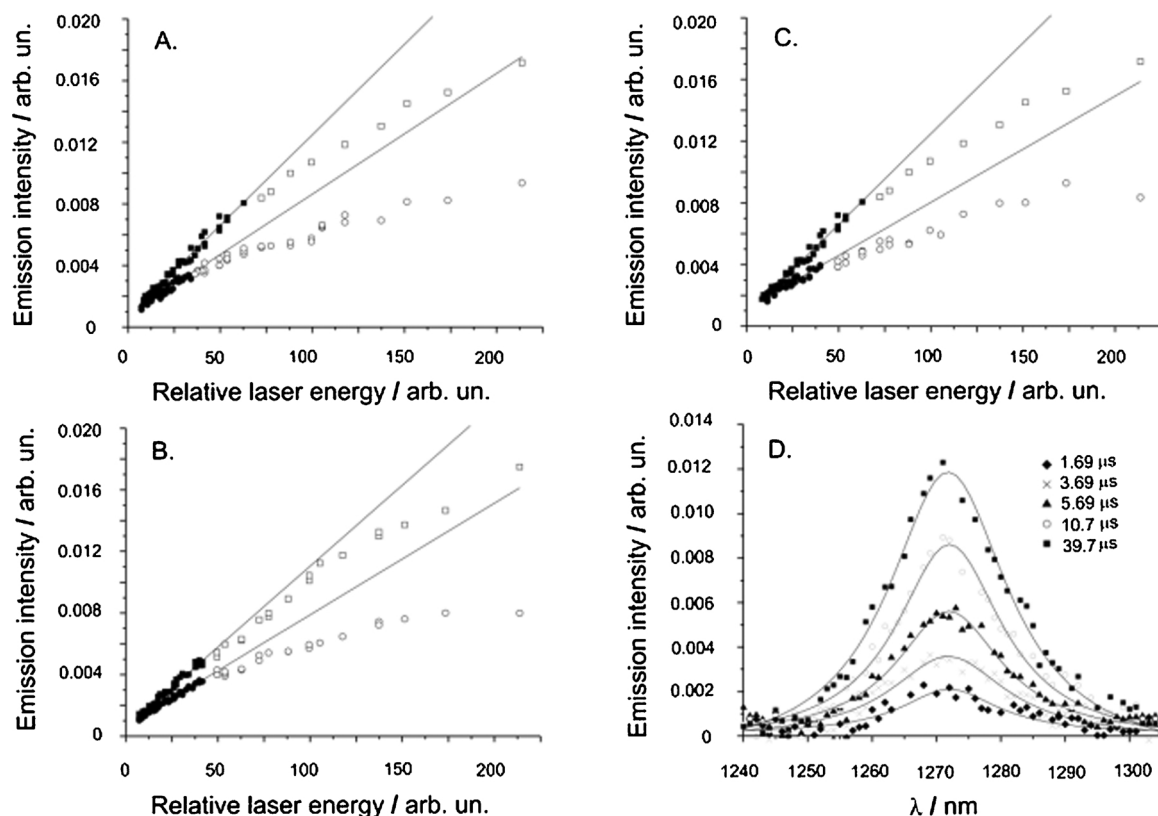


Fig. 2. Singlet oxygen emission intensity at 1271 nm vs. relative laser energy: squares (■/□) – phenalenone; circles (○/●) – chlorin e6 derivatives – chl ara 3 (A), chl mme 2 (B), chl glc 4 (C); As shown, function $y = ax + b$ was fitted only to the linear part of data; Filled symbols - linear part of data, blank symbols - nonlinear part of data. (D) Singlet oxygen phosphorescence spectrum measured for phenalenone.

Table 4

Photostability of chlorin e6 derivatives in DMSO (20 μ M) following irradiation with different red-light doses assessed as the ratio of absorbance for the most red-shifted Q band measured after (A) and before (A_0) exposure to the light.

Energy dose / J/cm^2	Exposure time / s	A / A_0 / %		
		chl ara 3	chl glc 4	chl mme 2
4.56	120	96.22	99.25	96.82
9.12	240	94.94	98.25	94.06
13.68	360	93.94	97.37	93.74
15.96	420	92.42	95.24	92.78
18.24	480	91.53	94.49	91.61
20.52	540	89.99	92.73	89.49
22.80	600	88.34	91.73	88.43

dose of 20 J/cm^2 used in biological *in vitro* experiments, the decrease in the intensity of the last Q band did not exceed 12 % (Table 4). This value seems to be adequate for PDT because, for example, Photodithazine®(PZ) (a noncovalent salt complex of chlorin e6 with N-methyl-D-glucosamine), which has received clinical approval in Russia, showed 9% intensity decrease in the 656 nm band (in PBS pH 7.4; irradiated at 630 nm) [50]. The photodegradation of all investigated chlorins was negligible despite their monomerisation, which was most evident for chl glc 4. As it is known, the studies of Verteporfin photobleaching showed that monomeric forms of photosensitizer are less "resistant" to the above phenomenon than aggregates [9]. Moreover, the modifications caused by exposure to the light include only band intensity changes. No disappearance or emergence of bands, which would indicate the formation of new photoproducts, was noted.

3.6. Size and polydispersity index (PDI) of differently charged liposomes

The idea of using nanoparticles as carriers of hydrophobic drugs in the bloodstream [51–56] can also be used to improve the effectiveness of photodynamic therapy. Therefore, it was examined whether the use of liposome carriers would improve the therapeutic effect of the PDT with selected chlorin derivatives on the basis of physicochemical and cytotoxic properties (chl ara 3 and chl mme 2). As both the value of charge and its density on the surface of liposomes affect their stability, biodistribution and the degree of accumulation in the cell [57,58], we proposed the use of three types of liposomes – neutral, anionic and cationic. Neutral liposomes are less removed by cells of the reticuloendothelial system (RES) and aggregate more strongly after systemic administration compared to other types of liposomes. Anionic liposomes are characterised by increased stability in suspension. In addition, the use of certain glycolipids, such as the monoganglioside GM1 or phosphatidylinositol PI, inhibits the uptake of these liposomes by macrophages and RES cells, which increases their circulation time in the bloodstream up to 12 h [59–61]. In contrast, cationic liposomes have a high ability to interact with serum proteins, which results in their increased uptake by RES. They are also proposed as a system for delivering substances to cells thanks to their fusion with the cell membrane [57,62–64].

In the first stage, the diameter of the tested liposomes and the values of the polydispersity index PDI were determined (see Table S1). For this purpose, the Zetasizer Nano ZS (Malvern) particle size analyzer was used.

The size of liposomes is one of the main parameters determining their distribution and removal from the body, because it affects the degree of uptake by macrophages and cells of the reticuloendothelial system [65,66]. Comparing the obtained diameter values of different types of empty liposomes, it was observed that liposomes containing

polyethylene glycol had the smallest size. The diameter of these liposomes did not exceed 120 nm. A slightly larger diameter of 125 nm has been observed in the case of DPPC/DPPG anionic liposomes (DPPC – 1,2-dipalmitoylphosphatidylcholine, DPPG – 1,2-dipalmitoylphosphatidylglycerol). In contrast, empty liposomes with cholesterol are over 15 nm larger than the others. Similarly, among liposomes with chl mme 2, those with cholesterol have the largest diameter. The sizes of liposomes with polyethylene glycol and DPPC/DPPG are similar to each other and do not exceed 127 nm. The smallest sizes of liposomes were observed for those with chl ara 3. However, the relationship between the sizes of individual types of liposomes is similar to that in previous groups. The smallest are liposomes with polyethylene glycol and DPPC/DPPG, their diameter ranges from 111 to 114.3 nm. HSPC/Chol (HSPC – 1- α -phosphatidylcholine, Chol – cholesterol) and HSPC/DOTAP/Chol liposomes (DOTAP – 1,2-dioleoyl-3-trimethylammonium-propane) are at least 12 nm larger than the others. Also, the polydispersity coefficient values obtained for all tested types of liposomes, both empty and with compound, are less than 0.14. According to the literature data, if the PDI value does not exceed 0.3, the obtained liposome suspension is homogeneous [67,68]. Due to the above, the obtained liposomes are characterised by a homogeneous size distribution.

Studies have shown that the uptake of liposomes by RES and their opsonization by plasma proteins increases with their diameter. However, the size reduction causes an increase in their accumulation in cancerous tissues. This effect may be associated with longer circulation time of smaller liposomes in the bloodstream and the fact that tumours are supplied by the leaking blood vessels, which also facilitates the accumulation of small liposomes in target tissues [57,61,62]. In photodynamic therapy, when photosensitizers are encapsulated in 100–400 nm liposome carriers, their passive tumour accumulation is optimised [52,60,69–71]. Therefore, the obtained liposomes are characterised by a suitable size, which helps to effectively deliver the photosensitizer to cancer cells.

3.7. Stability of liposomes

The modification of the liposome surface by the incorporation of small amounts of compounds possessing hydrophilic groups into the membrane composition may reduce their interactions with blood components and prevent their detection by the RES system [57,62,72]. As a consequence, liposomes of this type are more stable in the biological environment and may have an almost 10-fold longer half-life in the bloodstream [57,62]. Most often, phosphatidylethanolamine conjugated to the hydrophilic polymer polyethylene glycol (PEG) is used to obtain a hydrophilic coating around liposomes [59]. Depending on the length of the polymer, it forms an additional layer with a thickness of 5 nm around the liposome that does not affect the total value of the charge on the surface of the vesicles. Liposomes containing 2000 Da polyethylene glycol have the longest circulation time in the bloodstream [57,61,73–75]. On the other hand, the addition of cholesterol stiffening the bilayer to the composition of the liposome membrane makes it possible to reduce the leakage of the substance encapsulated in liposomes [71,74,76,77]. Thus, the composition of liposomes affects their stability and efficiency in drug delivery. Therefore, we examined the stability of different types of liposomes held for 28 days.

Based on the analysis of the size and PDI of liposomes stored at 3 °C for 28 days, it was found that the most stable are HSPC/Chol and HSPC/DSPE-PEG2000 liposomes, both empty and with chl mme 2 and chl ara 3 (see SI, Figures S9–17). Cationic and anionic liposomes with chl mme 2 and chl ara 3 should be prepared immediately before use because they show the least stability when stored at 3 °C, or they should be stored in freeze-dried form prior to using in order to avoid stability issues.

Table 5
Encapsulation efficiency of chlorins into liposomes (EE%).

Type of liposomes	EE [%] Chl mme 2	EE [%] Chl ara 3
HSPC/Chol (7:3)	89.83 ± 5.10	96.68 ± 2.07
HSPC/DSPE-PEG2000 (9.5:0.5)	82.03 ± 2.38	91.84 ± 0.87
HSPC/DOTAP/Chol (6:1:3)	89.19 ± 4.00	97.77 ± 5.80
HSPC/DOTAP/DSPE-PEG2000 (8.5:1:0.5)	91.20 ± 3.19	87.69 ± 7.27
DPPC/DPPG (9:1)	95.66 ± 5.54	90.17 ± 2.05
HSPC/DSPG/DSPE-PEG2000 (8.5:1:0.5)	92.90 ± 1.67	92.95 ± 4.17

3.8. Encapsulation efficiency of chlorins into liposomes (EE%)

Another important parameter when creating drug-transporting liposomes is the percentage of substance encapsulated in them. The effectiveness of drug incorporation in liposomes was determined on the basis of the ratio of photosensitizer concentration per 1 mg of phospholipids, before and after filtration on a column filled with Sephadex G-50 Fine cap (5.5 × 70 mm) (Table 5).

The encapsulation efficiency in liposomes for chl mme 2 and chl ara 3 is very high – over 80 % in the worst case (HSPC/DSPE-PEG₂₀₀₀ with chl mme 2–82.03 %; HSPC/DOTAP/DSPE-PEG₂₀₀₀ with chl ara 3–87.69 %). For chl mme 2, the highest efficiency was obtained for anionic liposomes DPPC/DPPG over 95 % and slightly lower 91–92 % for sterically stabilized liposomes (HSPC/DOTAP/DSPE-PEG₂₀₀₀ and HSPC/DSPG/DSPE-PEG₂₀₀₀). In the case of liposomes with chlorin, the highest efficiency (96 %) is characterised by those with cholesterol. Anionic liposomes and HSPC/DSPE-PEG₂₀₀₀ are characterised by chlorin encapsulation efficiency in the range of 90–93 %.

3.9. Biological *in vitro* studies

3.9.1. Cytotoxicity and phototoxicity

Human colon adenocarcinoma cells (HCT116 and HCT116 p53^{-/-}) were exposed to the PS alone, which permitted for dark cytotoxicity assessment, or both PS and light (at maximum absorption), which in turn allowed for evaluating their phototoxicity. No cytotoxic effects were observed in the dark in a broad range of concentrations. Following the light exposure, cell mortality increased along with the PS concentration (Fig. 3). Temoporfin was used as a control in these studies, and the experiments were carried out with cells bearing a wild-type or mutant (p53^{-/-}) p53 gene. The strongest cytotoxic effects were observed for chl ara 3. The chlorin chl mme 2 was found to be almost as effective as chl ara 3, particularly for HCT116 p53^{-/-} cells. Temoporfin was less effective, at least until 0.5 μ M concentration (Fig. 3). However, it should be remembered that the MTS test measures cell viability by analysing their metabolic activity (the activity of the mitochondrial dehydrogenase enzyme) and determining the number of cells with active mitochondria. However, clonogenic assay is considered to be the reliable standard because it exclusively answers the question of what percentage of cells capable of unlimited proliferation survives the treatment with a given compound. It cannot be excluded that in a longer period of time, after the stress factor has occurred, the damage can be repaired, or the cells considered alive in the MTS test may activate mechanisms leading to their death. To verify the results obtained with the MTS test, a clonogenic assay was performed to unequivocally assess the effects of therapy. Clonogenic assays revealed that chl ara 3 outperforms the remaining PS in HCT116 p53^{-/-} cells, and only at the highest concentrations, it shows lower anticancer activity in HCT116 cells compared to temoporfin (Fig. 4). IC₅₀ values were calculated based on the results and are shown in Table 6. This study investigates the susceptibility of wild-type and p53 knockout HCT116 cells. Mutations of the p53 tumour suppressor gene constitute one of the most frequent molecular changes in a wide variety of human

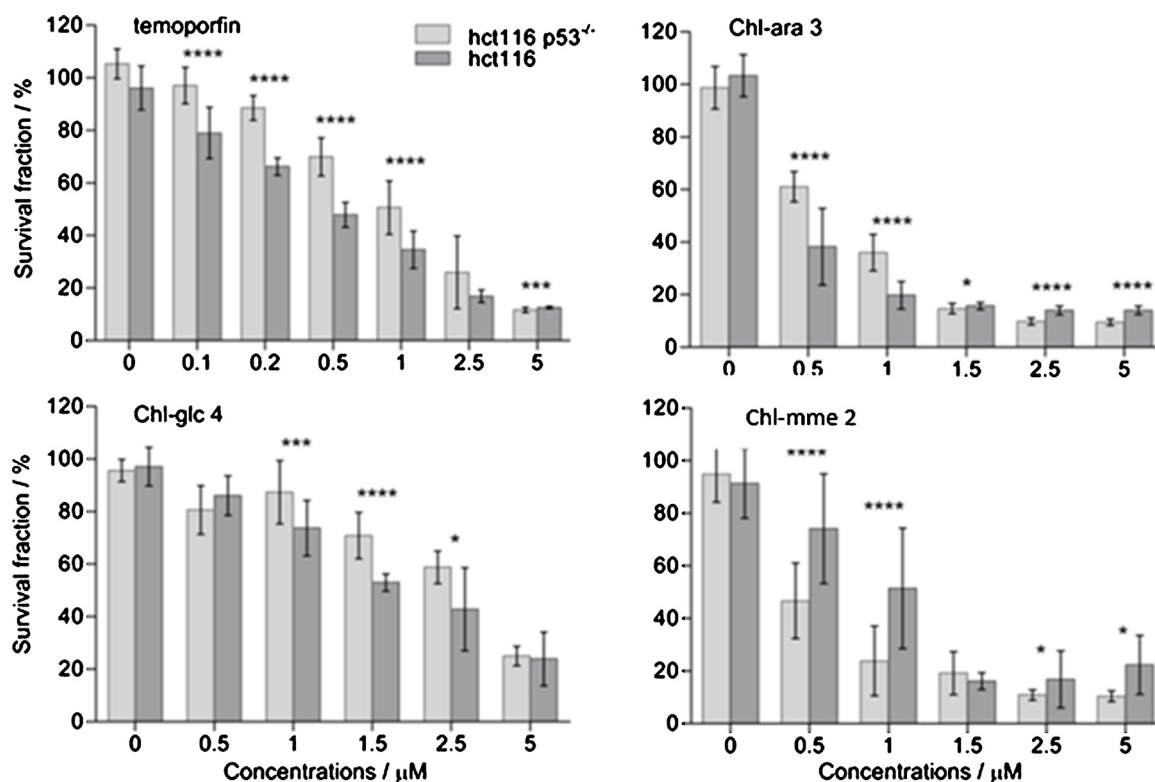


Fig. 3. Phototoxicity of temoporfin (Foscan, 5,10,15,20-tetra(m-hydroxyphenyl)chlorin), chl ara 3, chl glc 4 and chl mme 2 in HCT116 cells after 3-h incubation with compounds at different concentrations and illumination with red light (20 J/cm²) emitted by a halogen lamp (λ ≥ 630 nm). The survival fraction (% of control cells) was determined 24 h post irradiation using the MTS assay. The untreated and not irradiated cell population corresponds to 100 %. The results were obtained from at least three independent experiments in triplicate and presented as mean ± SD. Statistical significance was assessed using the Mann-Whitney test ****P < 0.0001; ***0.0001 < P < 0.001, **0.001 < P < 0.01; *0.01 < P < 0.05.

cancers. The p53 protein is a transcription factor that plays a major role in initiating the cell's response to stress factors, mainly DNA damage, hypoxia and abnormal proliferative signals. Cellular stress stabilizes the p53 protein and depending on how high the stress level is, the cell cycle is inhibited or cells that have been irreversibly damaged die in the process of apoptosis [78–80]. The results for compounds (chl ara 3 and chl glc 4) and temoporfin clearly show that for the HCT116 p53^{-/-} IC₅₀ values are higher in the MTS assay but lower in the clonogenic assay. Further research is necessary to determine the role of p53 in cell death as a result of photodynamic therapy.

3.9.2. Cellular chlorins retention kinetics

The kinetics of photosensitizer retention and elimination from the tumour cells are, from the clinical point of view, as important as their subcellular localization. Therefore, the location and final concentration of the photosensitizer inside cancer cells are crucial for the outcome of PDT. In order to confirm the penetration of the compounds into cancer

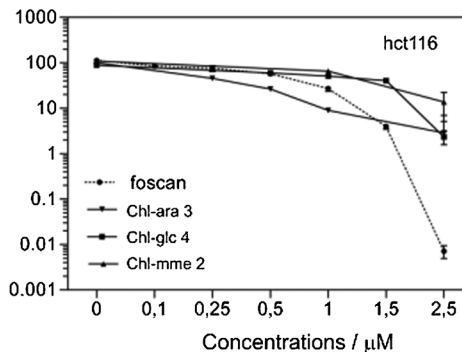
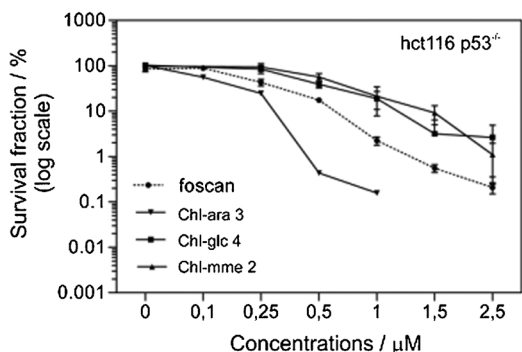


Fig. 4. Cell survival measured by clonogenic assay for HCT116 cells following PDT treatment (3-h incubation, irradiation 20 J/cm²) with chl ara 3, chl glc 4, chl mme 2 and temoporfin (as a reference compound). Each experiment was performed twice (mean ± SD). The concentration of 5 μM is not shown on the graphs because no colony was formed although all the treated cells were seeded.

Table 6
IC₅₀ values obtained for HCT116 cells following 3.5-h incubation with chlorins and red light irradiation (20 J/cm²). The results were obtained from at least three independent experiments in triplicate and presented as mean ± SD.

Compound	IC ₅₀ / μM			
	MTS assay		Clonogenic assay	
	HCT116 p53+/+	HCT116 p53-/-	HCT116 p53+/+	HCT116 p53-/-
chl ara 3	0.31 ± 0.03	0.50 ± 0.05	0.22 ± 0.03	0.12 ± 0.03
chl glc 4	2.08 ± 0.17	3.10 ± 0.42	0.83 ± 0.32	0.45 ± 0.08
chl mme 2	0.96 ± 0.12	0.37 ± 0.04	1.23 ± 0.30	0.58 ± 0.06
temoporfin	0.45 ± 0.03	1.04 ± 0.11	0.51 ± 0.13	0.23 ± 0.02

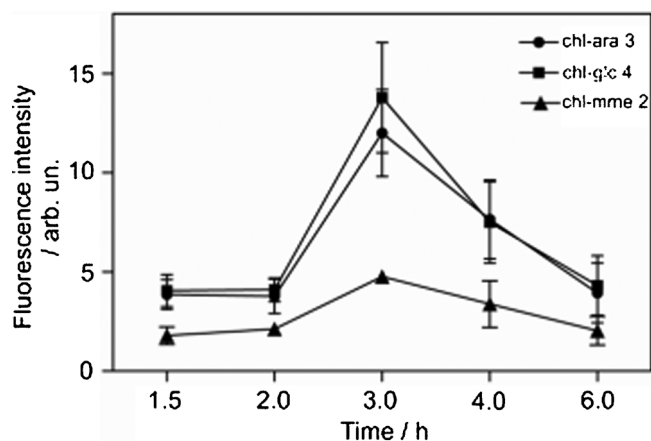


Fig. 5. The kinetics of photosensitizer (2.5 μ M) uptake (HCT116 cells) assessed by spectrophotometric measurement of cell lysates. Each time point is an average of eight experimental points (mean \pm SD).

cells, we performed experiments with lysates of cells, which were previously incubated with particular chlorins. In the first stage, three-dimensional charts of emission vs. excitation were recorded. The occurrence of the additional band (invisible for the control group) corresponds to the presence of chlorin. It was concluded that the emission bands obtained for the lysates after 3 h had the highest intensity (see Figure S18).

The optimal incubation time was confirmed by time-dependent fluorescence measurements after the PS excitation at a wavelength corresponding to the maximum of Soret band (for 1, 2, 3, 4 and 6 -h incubation). The correlation between the maximal fluorescence intensity (as well as the accumulation rate) and the time of incubation was estimated (Fig. 5). The optimal incubation time was between 3 and 4 h, depending on the chlorin. For chlorin chl glc 4, the maximum was visible after three hours. For the remaining chlorins (chl ara 3 and chl mme 2), the difference in their concentration inside the cells was not as evident. Therefore, the optimal incubation time of 3 h was chosen for chl ara 3 and chl mme 2.

3.9.3. Subcellular localization of photosensitizers

As it is essential to ensure the effectiveness of PDT, the accumulation of the photosensitizer at the specific site of the cancer cells is desirable. Many reports have implicated mitochondria and lysosomes as important PDT targets. The localization in mitochondria is reported to be more efficient in killing cells than the localization at other cellular sites [81]. The preference for membrane or other cellular compartment localization is related to different photosensitizer properties. Photosensitizers (frequently hydrophobic) penetrate membranes and damage them, which in most cases results in necrosis. Those compounds accumulating in the cytoplasm of the eukaryotic cells (especially hydrophilic) initiate apoptosis. However, the process of photosensitizer accumulation in the cells and the associated therapeutic efficacy is much more complex. Even if various photosensitizers accumulate in the same organelles, their effectiveness may differ due to, for instance, their different tendency to aggregate. Therefore, small changes in PS physicochemical properties affect their specific or non-specific tissue binding ability, which obviously changes the subcellular location of the photosensitizer and the way it acts. Additionally, this effect is specific both to particular cell lines and to the applied incubation protocol.

To determine subcellular chl ara 3, localization fluorescence microscopy was used with PS together with MitoTracker, ERTracker, LysoTracker and/or Hoechst reagent. After only 2 h, all cells incorporated the PS and showed intense bright-red fluorescence originating from the internalized compound (Fig. 6). In no cases did the photosensitizer accumulate inside the cell nucleus. Therefore, the risk

of DNA damage during PDT seems to be small. The double staining group with chlorin and MitoTracker revealed that chl ara 3 localizes to some extent in mitochondria, but there are some areas with only red fluorescence representing chlorin still situated in other compartments of the cell. Staining with chlorin and ERTracker as well as chlorin with LysoTracker indicated that chlorin penetrated endoplasmic reticulum and lysosomes successfully.

The limitation relating to the fluorescence microscope is that the image reaching the detector comes not only from the focus plane, because the lens of the microscope collects light from the entire cross-section of the sample. In addition, the emission filters used in wide-field microscopy can cause that fluorescence from two different fluorescence markers can partially overlap, making correct analysis difficult. Both of these problems are eliminated when a confocal microscope is used for imaging. Therefore, intracellular localization of chlorin ara 3 was verified using a Zeiss LSM 700 confocal microscope and ZEN 2.1 software (see Figure S19 in SI).

3.9.4. Morphological changes in tumour cells undergoing PDT

Photodynamic therapy, also *in vitro*, leads to cell death via apoptosis, necrosis and autophagy [82,83]. To obtain insight into morphological changes induced in tumour cells by investigated PS, phase contrast, light and scanning electron microscopy (cryo-SEM) observations were carried out. These experiments revealed that PDT with chl ara 3 leads to a rapid (within 6 h) and robust (observed already at 0.5 μ M concentration) shrinkage and detachment of cells accompanied by extensive plasma membrane blebbing (Fig. 7), typically observed during its damage and leading to necrosis. Similar changes were observed when temoporfin was used in PDT, but both detachment and blebbing were observed at higher PS concentrations. Also, cryo-SEM observations of HCT116 cells undergoing PDT with chl ara 3 revealed marked and irregular lesions in the plasma membrane of the treated cells (Fig. 8). Moreover, phase-contrast microscopic observations showed that PDT with chl ara 3 led to extensive cytoplasmic vacuolation, typical for necrosis (Fig. 9B). Tumour cell necrosis is associated with the development of extensive inflammatory response that may stimulate adaptive immunity against residual or metastatic malignant cells, which may contribute to the effectiveness of the therapy [84]. However, it should be emphasized that one compound may induce necrosis and/or apoptosis depending on experimental conditions. Apparently, treatment success does not exclusively depend on the induction of only one type of cell death, especially in solid tumours [55]. The desirability of apoptotic vs. necrotic cell death and optimal apoptosis/necrosis ratio is still unclear. Bruin et al. discussed this problem extensively [85]. Therefore, the applied treatment protocol should mostly guarantee, through optimal apoptosis/necrosis ratio, the safety and efficiency of the therapy. In future studies, we will attempt to confirm our preliminary distinction between apoptosis, necrosis and autophagy through biochemical analyses (e.g. caspase activation, markers analysis – Annexin V/propidium iodide staining).

3.9.5. Toxicity of liposomes

Liposomal carriers are perfectly suited for the transport of drugs, because by modifying their size, charge and the composition of the phospholipid membrane, in addition to increasing the accumulation of the drug in cancer cells, they provide a significant reduction in drug concentration in healthy tissues, and thus a significant reduction in the toxicity of therapeutic agents [56,65,72,86]. The composition and size of liposomes must, however, be selected so that the carriers themselves neither pose a hazard nor show toxicity.

The obtained MTS test results confirm that both empty liposomes (see Figure S20) and those in which chlorins have been encapsulated (see Figure S21 and Figure S22), in the absence of light, do not show a toxic effect on HCT116 cells. Only slight decreases of a few percent in cell survival were observed. The largest decrease in cell survival by approximately 12 % was observed for HSPC/DSPE-PEG2000 liposomes

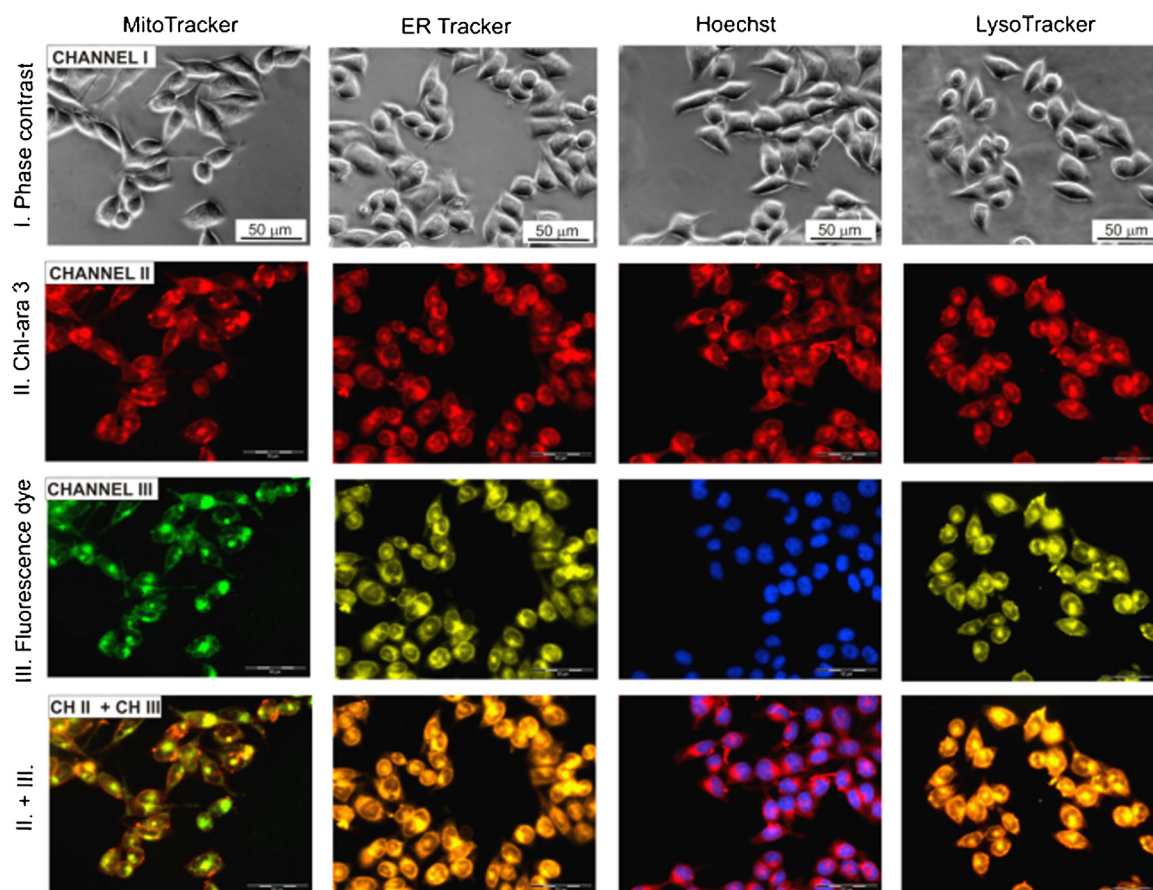


Fig. 6. Subcellular localization of chl ara 3 (2.5 μM) following 2-h incubation and staining with fluorescence dyes – MitoTracker (100 nM, 30 min), ERTracker (1 μM , 1 h), Hoechst (4 $\mu\text{g}/\text{mL}$, 30 min) and LysoTracker (5 μM , 1 h).

with chl mme 2.

3.9.6. Liposome carriers in chlorin-PDT therapy

In the next stage, the photodynamic effect of the tested liposome-drug complexes was assessed in comparison to the effect obtained for the photosensitizer alone. The assessment of the viability of cells incubated with photosensitizers encapsulated in liposome carriers or treated with free photosensitizer and exposed to light was performed based on statistical analysis using a non-parametric Mann-Whitney U test. The statistical analysis was performed using Statistica (version 10). Normal distribution was verified using the Shapiro-Wilk test.

It was observed that at each chlorin concentration, greater photodynamic effects were obtained for the tested liposomal formulations (Fig. 10a). For example, for the lowest tested concentration and a light dose of 4.2 J/cm^2 , cell viability is 1.7 (HSPC/DOTAP/Chol) to 2.5 (DPPC/DPPG) times less compared to the chl mme 2 itself. DPPC/DPPG liposomes at a concentration of 2.5 μM chl mme 2 caused up to 61 times higher cell mortality than the compound alone (Fig. 10a). Also, a strong photodynamic effect of chl mme 2 in liposomal formulations was observed for a light dose of 12.5 J/cm^2 (Fig. 10b). The largest differences in cell viability were observed for DPPC/DPPG liposomes at a concentration of 0.5 μM and 1 μM , compared to chl mme 2 alone. For these liposomes, cell viability was 15 and 28 times lower, respectively, than after the application of the free photosensitizer.

The viability of cells treated with HSPC/DOTAP/DSPE-PEG₂₀₀₀ liposomes with chl ara 3 is 4.2–10 times lower, depending on the concentration of 0.5 μM – 1 μM , than that of cells which survived irradiation after incubation with the compound itself (Fig. 10c). For higher concentrations of chl ara 3, the differences between the cell viability obtained for individual types of liposomes are no longer as pronounced.

The best photodynamic effect was obtained for HSPC/Chol liposomes with chl ara 3 at 0.5 μM concentration and a light dose of 12.5 J/cm^2 . In this case, the cell viability was 42 times lower than that obtained for free chlorin (Fig. 10d).

4. Discussion

The antitumour effectiveness of PDT depends on the photophysical and chemical properties (charge, hydrophilicity/ hydrophilicity, the tendency for aggregation) of the photosensitizers as well as their chemical structure (type, number and the quantity of substituents and functional groups, the presence of rings and the central atom) [87,88]. Therefore, we firstly explored the photophysical properties of the compounds. The analysis of the investigated chlorins revealed typical features of absorption and emission spectra, including high values of molar absorption coefficients for the last Q band, which guarantees efficient molecule excitation. The assessed values of fluorescence quantum yields were 0.24–0.27. The photodegradation of the investigated chlorins was negligible despite their monomerisation. Chlorin chl glc 4 was the most stable.

The obtained triplet state lifetimes were in the range of 0.23–0.27 μs , which was comparable to the value referred to in the literature [42]. The singlet oxygen quantum yields of chl ara 3 (0.63) and chl mme 2 (0.66) were comparable. The lowest value was obtained for chl glc 4 (0.56). Thus, all the chlorins also had relatively high (above 50 %) quantum yields of singlet oxygen generation. The obtained results are comparable to the literature value of $\Phi\Delta$ for chlorin e6 [42,45]. To summarize, the photophysical properties of new chlorin e6 derivatives meet the necessary requirements to be applied in PDT.

It was concluded that the emission bands obtained for the lysates

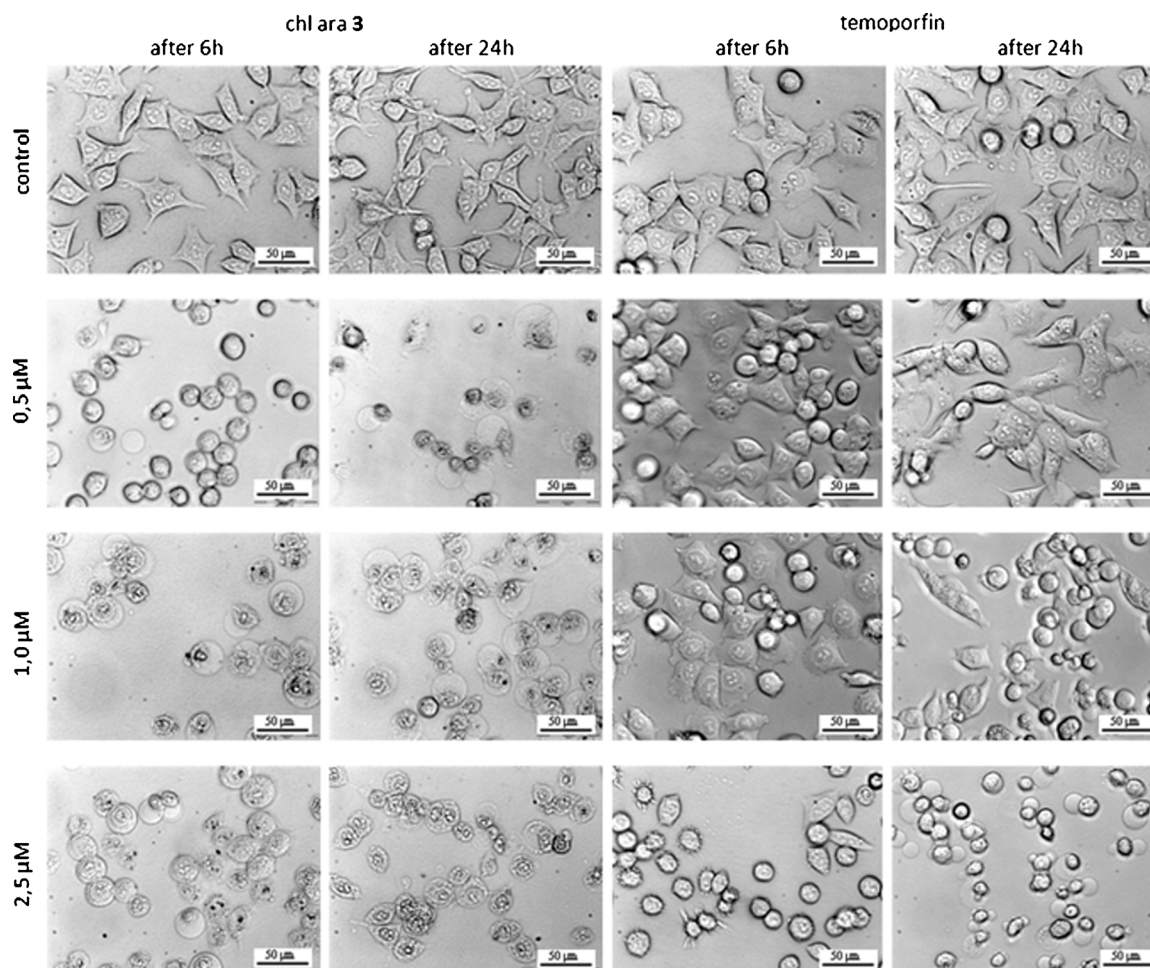


Fig. 7. Light microscopic images of HCT116 control cells (no light, no photosensitizer) and HCT116 cells following 3.5-h incubation with chl ara 3 or temporfin and subsequent red-light irradiation (20 J/cm^2). Image recording was performed 6- and 24-hs post irradiation. Treated cells have a different morphology compared to the control cells. Among the treated cells, swollen cells were observed (similar to necrotic cells). Apoptotic cells exhibit a rather shrunken morphology.

after 3 h had the highest intensity. This might indicate that after such a period of time, the concentration inside the cells was maximal, which proves the efficient transportation of chlorins into the cells.

The evaluation of the biological mechanisms of action of new derivatives consisted first of all in determining the time at which the compounds penetrate into the cells. Our compounds localized very efficiently in the lysosomes, endoplasmic reticulum (ER), mitochondria and cytoplasm. Importantly, chl ara 3 failed to localize in the cell nucleus, thereby minimizing potential mutagenic effects resulting from DNA damage.

Our research indicates a lack of dark cytotoxicity in the selected range of photosensitizer concentrations, as well as excellent photodynamic efficiency. MTS and clonogenic assays results have shown that all chlorins had a strong cytotoxic effect in HCT116 cells.

PDT with our compounds resulted in significant morphological cell changes. The cells immediately showed extensive damage which increased with the higher concentration of photosensitizer and the longer post-irradiation time. Electron microscopy found that the cell membranes were strongly damaged and the cellular components leaked out. Therefore, these compounds seem to induce necrosis.

Our study also proved that the use of liposomes to transport new chlorin e6 derivatives improves the effectiveness of PDT therapy. The diameters of liposomes tested did not exceed 170 nm, so their size would be suitable for transporting drugs to the tumour through the leaking blood vessel system [34,89]. It is known that liposomes between 50 and 200 nm proved to be clinically useful as they lose less

drugs and do not undergo phagocytosis. It was found that the liposomes HSPC/Chol and HSPC/DSPE-PEG₂₀₀₀ are stable for 28 days, both empty and with chl mme 2 and chl ara 3. The encapsulation efficiency in liposomes for chl mme 2 and chl ara 3 is very high – in most cases exceeding 90 %. The obtained MTS test results confirm that both empty liposomes and those in which chlorins have been encapsulated, in the absence of light do not show toxic effect on HCT116 cells. The therapeutic effect of chlorins encapsulated in liposomes has been shown to be much stronger than when given free compounds. The largest differences in the cell viability were observed for DPPC/DPPG liposomes with chlorin at a concentration of 0.5 and 1 μM (15 and 28 times lower), compared to chl mme 2 alone.

For chl ara 3, efficacy was improved, depending on the liposome type and dose, from 4.2–42 times relatively to the effect obtained for the free compound. HSPC/Chol liposomes provided the best therapeutic effect. In conclusion, the amidation of chlorin e6 with a sugar derived from amino polyols is an excellent tool to improve the therapeutic effectiveness of PDT.

The hydrophilicity of PS is a barrier, which hinders their passing through the lipid bilayer resulting in their poor cellular uptake. Highly lipophilic photosensitizers can easily permeate membranes, but they do not easily dissolve in aqueous media. In order to improve solubility, functionalization such as sulphonation is normally used, but this alters other characteristics, perhaps deleteriously. Here we show that the use of non-ionic polyol amide derivatives to enhance the delivery of primary hydrophobic compounds to tumours appeared to be an excellent

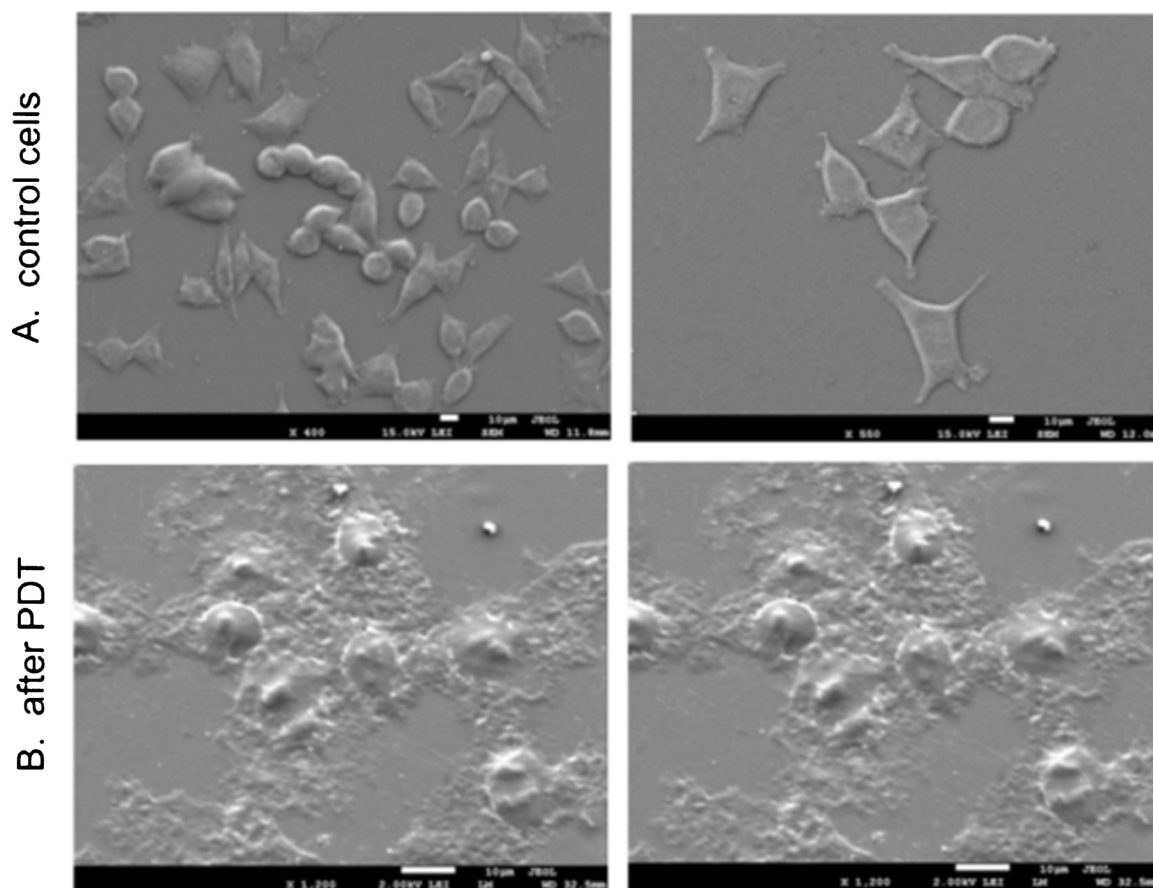


Fig. 8. Cryo-SEM images of HCT116 cells. Control cells (no photosensitizer) (A); Cells incubated with chl-ara 3 (2.5 μM) following red light irradiation (20 J/cm^2) (B). Microscope analysis was performed 24 h post irradiation.

alternative to other methods. The chlorin e6 glyco-derivatives had sufficient photophysical properties (they do not aggregate or photobleach, but can be effectively excited and successfully generate singlet oxygen). They acted *via* multiple rather than singular sites within the target cell, thus indicating high photodamage and necrotic cell death. The observed lack of dark toxicity and mutagenicity, as well as higher than temoporfin photodynamic efficacy, make new chlorins e6 derivatives promising candidates for PDT applications.

5. Conclusions

An ongoing trend in photodynamic therapy is to increase the selectivity of photosensitizers by effecting a significantly higher concentration in cancerous tissues. New photosensitizers are being sought

and attempts made to modify the already tested photosensitizers to increase efficiency, broaden indications and eliminate the side effects of PDT. In our work, we succeeded in proving that glycosylated derivatives of e6 chlorins exhibit beneficial physicochemical properties as well as increased anti-tumour efficacy when administered in liposome carriers. This gives hope for future research using these compounds and targeted media.

Declaration of Competing Interest

There are no conflicts to declare.

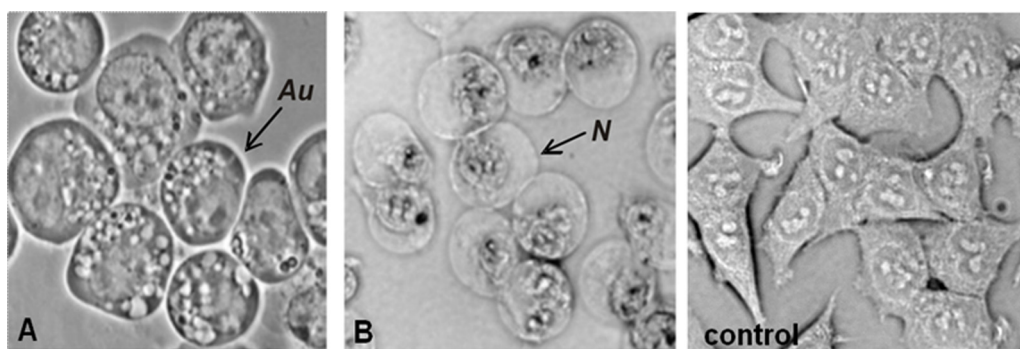


Fig. 9. Phase-contrast microscopic image of autophagy (Au) in murine leukemia cells (L1210/Bax) after PDT(A) [52]. Phase-contrast microscopic image of HCT 116 cells treated with 1 μM of chl-ara 3 recorded 24 h post irradiation (fragment of image) (B). Necrotic cell death (N).

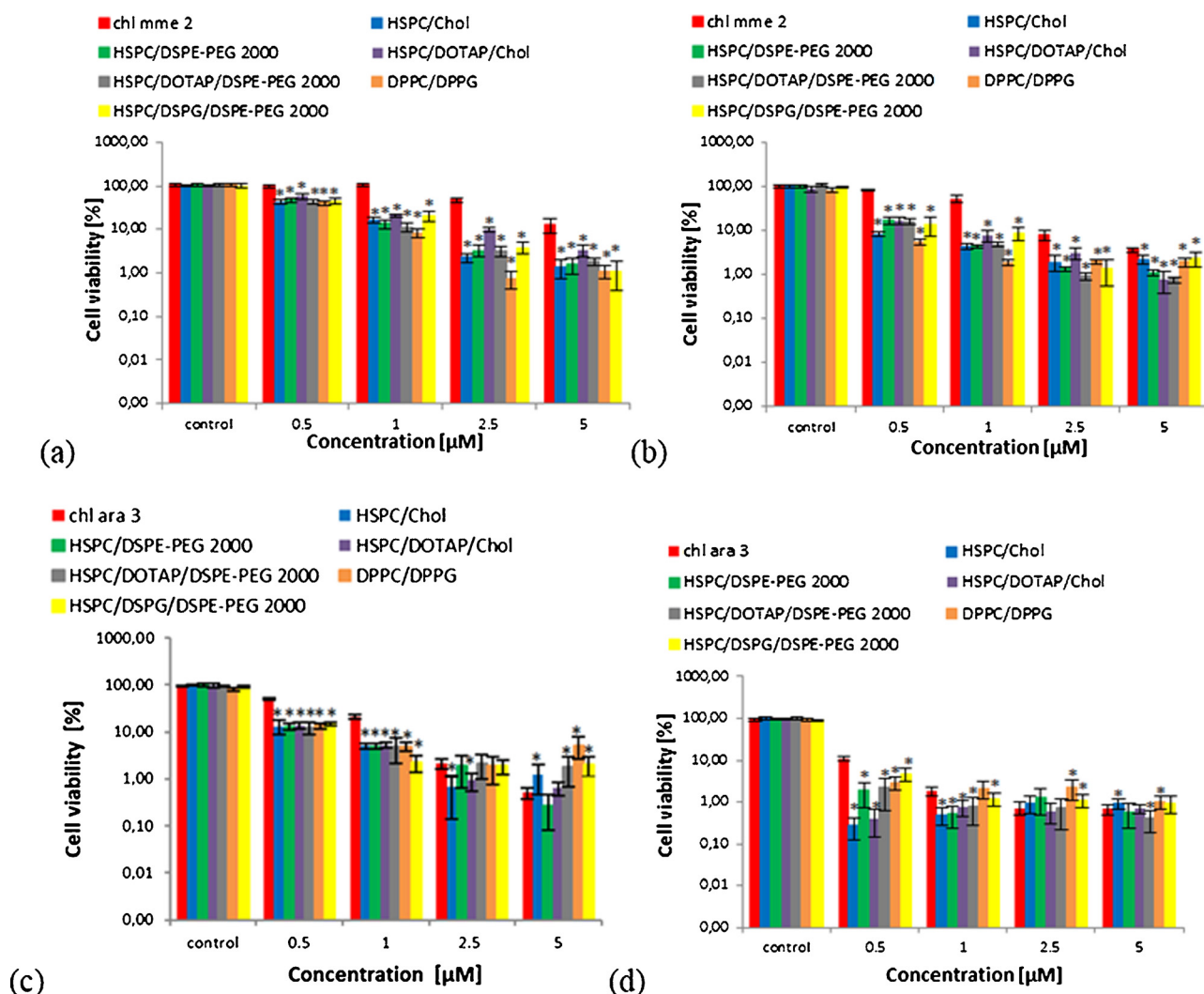


Fig. 10. Cell viability of HCT116 cells assessed by MTS assay after 4 h of treatment with (a) chl mme 2 and its liposomal formulations and a light dose 4.2 J/cm^2 ; (b) chl mme 2 and its liposomal formulations and a light dose 12.5 J/cm^2 ; (c) chl ara 3 and its liposomal formulations and a light dose 4.2 J/cm^2 ; (d) chl ara 3 and its liposomal formulations and a light dose 12.5 J/cm^2 . The results were obtained from three independent experiments in triplicate and presented as mean \pm SD. The differences between the analysed variables were considered statistically significant when the p value < 0.05 . Statistically significant differences are marked by asterisks*.

Acknowledgements

Marzena Rams-Baron and Patrycja Kozub acknowledge scholarships from the TWING project co-financed by the European Social Fund.

Gratitude to Dr Gabriela Kramer-Marek from The Institute of Cancer Research (London) for enabling research on confocal microscope during Dr Szurko's internship at ICR.

Appendix A. Supplementary data

Supplementary material related to this article can be found, in the online version, at doi:<https://doi.org/10.1016/j.pdpdt.2020.101799>.

References

- [1] M. Wainwright, Photosensitizers in Biomedicine, John Wiley and Sons, Chichester, 2009.
- [2] K. Lang, J. Mosinger, D.M. Wagnerová, Photophysical properties of porphyrinoid sensitizers non-covalently bound to host molecules: models for photodynamic therapy, *Coord. Chem. Rev.* 248 (2004) 321–350.
- [3] M. Ethirajan, Y. Chen, P. Joshi, R.K. Pandey, The role of porphyrin chemistry in tumor imaging and photodynamic therapy, *Chem. Soc. Rev.* 40 (2011) 340–362.
- [4] R. Bonnett, Chemical Aspects of Photodynamic Therapy By Raymond Bonnett, Gordon and Breach Science Publishers, Amsterdam, 2000.
- [5] P. Agostinis, K. Berg, K.A. Cengel, T.H. Foster, A.W. Girotti, S.O. Gollnick, S.M. Hahn, M.R. Hamblin, A. Juzeniene, D. Kessel, M. Korbelik, J. Moan, P. Mroz, D. Nowis, J. Piette, B.C. Wilson, J. Golab, Photodynamic therapy of cancer: an update, *CA-Cancer J. Clin.* 61 (2011) 250–281.
- [6] T.J. Dougherty, C.J. Gomer, B.W. Henderson, G. Jori, D. Kessel, M. Korbelik, J. Moan, Q. Peng, Photodynamic therapy, *J. Natl. Cancer Inst.* 90 (1998) 889–905.
- [7] A. Graczyk, Ch.1-2, Photodynamic Diagnosis and Treatment of Cancer, (1999), pp. 21–159 (in Polish).
- [8] A. Sieroń, W. Stręk, Diagnostics and Photodynamic Therapy, Wydawnictwo Medyczne Urban & Partner, Wrocław, 2004, pp. 1–32 (in Polish).
- [9] R. Bonnett, G. Martínez, Photobleaching of sensitizers used in photodynamic therapy, *Tetrahedron* 57 (2001) 9513–9547.
- [10] V. Cuomo, G. Jori, B. Rihter, M.E. Kenney, M.A.J. Rodgers, Liposome-delivered Si (IV)-naphthalocyanine as a photodynamic sensitizer for experimental tumours: pharmacokinetic and phototherapeutic studies, *Br. J. Cancer* 62 (1990) 966–970.
- [11] R.K. Pandey, G. Zheng, The Porphyrin Handbook Volume 6 (2000), pp. 158–163.
- [12] M.C. DeRosa, R.J. Crutchley, Photosensitized singlet oxygen and its applications, *Coord. Chem. Rev.* 233–234 (2002) 351–371.
- [13] F. Ricchelli, Photophysical properties of porphyrins in biological membranes, *J. Photochem. Photobiol. B, Biol.* 29 (1995) 109–118.
- [14] A. Kamkaew, L. Cheng, S. Goel, H.F. Valdovinos, T.E. Barnhart, Z. Liu, W. Cai, Cerenkov radiation induced photodynamic therapy using chlorin e6-Loaded hollow mesoporous silica nanoparticles, *ACS Appl. Mater. Interfaces* 8 (40) (2016) 26630–26637.
- [15] L. Cheng, A. Kamkaew, H. Sun, D. Jiang, H.F. Valdovinos, H. Gong, C.G. England, S. Goel, T.E. Barnhart, W. Cai, Dual-Modality Positron Emission Tomography/Optical Image-Guided Photodynamic Cancer Therapy with Chlorin e6-Containing

- Nanomicelles, *ACS Nano* 10 (8) (2016) 7721–7730.
- [16] S. Näkki, J.O. Martinez, M. Evangelopoulos, W. Xu, V.-P. Lehto, E. Tasciotti, Chlorin e6 functionalized theranostic multistage nanovectors transported by stem cells for effective photodynamic therapy, *ACS Appl. Mater. Interfaces* 9 (28) (2017) 23441–23449.
- [17] S.-R. Lee, Y.-J. Kim, Hydrophilic chlorin e6-Poly(amidoamine) dendrimer nanoconjugates for enhanced photodynamic therapy, *Nanomaterials* 8 (6) (2018) 445.
- [18] K.-H. Choi, K.C. Nam, G. Cho, J.-S. Jung, B.J. Park, Enhanced photodynamic anticancer activities of multifunctional magnetic nanoparticles (Fe3O4) conjugated with chlorin e6 and folic acid in prostate and breast Cancer cells, *Nanomaterials* 8 (9) (2018) 722.
- [19] R.G. Jinadasa, Z. Zhou, M.G. Vicente, K.M. Smith, Syntheses and cellular investigations of di-aspartate and aspartate-lysine chlorin e(6) conjugates, *Org. Biomol. Chem.* 14 (3) (2016) 1049–1064.
- [20] H. Chen, S.W. Humble, R.G.W. Jinadasa, Z. Zhou, A.L. Nguyen, M.G.H. Vicente, K.M. Smith, Syntheses and PDT activity of new mono- and di-conjugated derivatives of chlorin e6, *J. Porphyr. Phthalocyanines* 21 (4-6) (2017) 354–363.
- [21] M. Liu, C.-Y. Chen, A.K. Mandal, V. Chandrashaker, R.B. Evans-Storms, J.B. Pitner, D.F. Bocian, D. Holten, J.S. Lindsey, Bioconjugatable, PEGylated hydroporphyrins for photochemistry and photomedicine, Narrow-band, red-emitting chlorins, *New J. Chem.* 40 (2016) 7721–7740.
- [22] S. Kimani, G. Ghosh, A. Ghogare, B. Rudshteyn, D. Bartusik, T. Hasan, A. Greer, Synthesis and characterization of mono-, di-, and tri-poly(ethylene glycol) chlorin e6 conjugates for the photokilling of human ovarian cancer cells, *J. Org. Chem.* 77 (23) (2012) 10638–10647.
- [23] I. Laville, T. Figueiredo, B. Looock, et al., Synthesis, cellular internalization and photodynamic activity of glucoconjugated derivatives of tri and tetra(meta-hydroxyphenyl)chlorins, *Bioorg. Med. Chem.* 11 (2003) 1643–1652.
- [24] I. Laville, S. Pigaglio, J.C. Blais, et al., Photodynamic efficiency of diethylene glycol-linked glycoconjugated porphyrins in human retinoblastoma cells, *J. Med. Chem.* 49 (2006) 2558–2567.
- [25] S. Ballut, A. Makky, B. Chauvin, et al., Tumor targeting in photodynamic therapy. From glycoconjugated photosensitizers to glycodendrimeric one. Concept, design and properties, *Org. Biomol. Chem.* 10 (2012) 4485–4495.
- [26] M. Obata, S. Hirohara, K. Sharyo, et al., Sugar-dependent photodynamic effect of glycoconjugated porphyrins: a study on photocytotoxicity, photophysical properties and binding behavior to bovine serum albumin (BSA), *Biochim. Biophys. Acta* 1770 (2007) 1204–1211.
- [27] C.F. Choi, J.D. Huang, P.C. Lo, W.P. Fong, D.K. Ng, Glycosylated zinc(II) phthalocyanines as efficient photosensitizers for photodynamic therapy. Synthesis, photophysical properties and in vitro photodynamic activity, *Org. Biomol. Chem.* 6 (2008) 2173–2181.
- [28] J.T.C. Wojtyk, R. Goyan, E. Gudgin-Dickson, R. Pottier, Exploiting tumour biology to develop novel drug delivery strategies for PDT, *Med. Laser Appl.* 21 (2006) 225–238.
- [29] A. Mrozek-Wilczkiewicz, K. Malarz, M. Rams-Baron, M. Serda, D. Bauer, F.-P. Montforts, A. Ratuszna, T. Burley, J. Polanski, R. Musiol, Iron Chelators and Exogenic Photosensitizers. Synergy through Oxidative Stress Gene Expression, *J. Cancer* 8 (11) (2017) 1979–1987.
- [30] C.J. Monteiro, M.M. Pereira, M.E. Azenha, et al., A comparative study of water soluble 5,10,15,20-tetrakis (2,6-dichloro-3-sulphophenyl)porphyrin and its metal complexes as efficient sensitizers for photodegradation of phenols, *Photochem. Photobiol. Sci.* 4 (2005) 617–624.
- [31] R. Schmidt, C. Tanielian, R. Dunsbach, C. Wolff, Phenalenone, a universal reference compound for the determination of quantum yields of singlet oxygen $O_2(^1\Delta_g)$ sensitization, *J. Photochem Photobiol Chem.* 79 (1994) 11–17.
- [32] F.A. Schaberle, Assessment of the actual light dose in photodynamic therapy, *Photodiagnosis Photodyn. Ther.* 23 (2018) 75–77.
- [33] M. Legut, D. Lipka, N. Filipczak, A. Piwoni, A. Kozubek, J. Gubernator, Anacardic acid enhances the anticancer activity of liposomal mitoxantrone towards melanoma cell lines – in vitro studies, *Int. J. Nanomedicine* 9 (2014) 653–668.
- [34] A. Kozubek, Introduction to Liposome Technology, University of Wrocław Publishing House, 2004, p. 13 (in Polish).
- [35] S. Sur, R. Pagliarini, F. Bunz, C. Rago, L.A. Diaz, K.W. Kinzler, et al., A panel of isogenic human cancer cells suggests a therapeutic approach for cancers with inactivated p53, *Proc. Natl. Acad. Sci.* 106 (10) (2009) 3964–3969.
- [36] G. Kramer-Marek, C. Serpa, A. Szurko, M. Widel, A. Sochanik, M. Snietura, P. Kus, R.M. Nunes, L.G. Arnaut, A. Ratuszna, Spectroscopic properties and photodynamic effects of new lipophilic porphyrin derivatives: efficacy, localisation and cell death pathways, *J. Photochem. Photobiol. B* 84 (2006) 1–14.
- [37] K.M. Smith, D.A. Goff, D.J. Simpson, The meso substitution of chlorophyll derivatives: direct route for transformation of bacteriochlorophylls d into bacteriochlorophylls c, *J. Am. Chem. Soc.* 107 (1985) 4946–4954.
- [38] F.P. Montforts, D. Bauer, De 102010056443 a, (2012), p. 1.
- [39] D. Bauer, H.V. Nghiem, D.D. Tien, J. Stelten, F.P. Montforts, Functionalization of chlorin e6 trimethylester towards potential amphiphilic photosensitizers for photodynamic therapy, *J. Porphyrins Phthalocyanines* 23 (2019) 243–250.
- [40] J.B. Conant, K.F. Armstrong, Studies in the Chlorophyll Series. X. The Esters of Chlorin e, *J. Am. Chem. Soc.* 55 (1933) 829–839.
- [41] L.B. Josefsen, R.W. Boyle, Photodynamic therapy and the development of metal-based photosensitizers, *Met. Drugs* 276109 (2008) 1–24.
- [42] E. Zenkevich, E. Sagun, V. Knyukshko, et al., Photophysical and photochemical properties of potential porphyrin and chlorin photosensitizers for PDT, *J. Photochem Photobiol B.* 33 (1996) 171–180.
- [43] E.F.F. Silva, C. Serpa, J.M. Dąbrowski, Mechanisms of singlet-oxygen and superoxide-ion generation by porphyrins and bacteriochlorins and their implications in photodynamic therapy, *Chem. Eur. J.* 16 (9273-) (2010) 9286.
- [44] F. Wilkinson, W.P. Helman, A.B. Ross, Quantum yields for the photosensitized formation of the lowest electronically excited singlet state of molecular oxygen in solution, *J. Phys. Chem. Ref. Data* 22 (1993) 113–262.
- [45] R.W. Redmond, J.N. Gamlin, A compilation of singlet oxygen yields from biologically relevant molecules, *Photochem. Photobiol.* 70 (1999) 391–475.
- [46] R.V. Bensasson, E.J. Land, T.G. Truscott, Excited States and Free Radicals in Biology and Medicine, Oxford University Press, Oxford, New York, 1993.
- [47] Y. Hongying, W. Fuyuan, Z. Zhiyi, Photobleaching of chlorins in homogeneous and heterogeneous media, *Dye. Pigment.* 43 (1999) 109–117.
- [48] J.D. Spikes, J.C. Bommer, Photobleaching of mono-1-aspartyl chlorin e6 (NPe6): a candidate sensitizer for the photodynamic therapy of tumors, *Photochem. Photobiol.* 58 (1993) 346–350.
- [49] W.G. Roberts, K.M. Smith, J.L. McCullogh, M.W. Berns, Skin photosensitivity and photodestruction of several potential photodynamic sensitizers, *Photochem. Photobiol.* 49 (1989) 431–438.
- [50] C. Bernal, A.O. Ribeiro, G.P. Andrade, J.R. Perussi, Photodynamic efficiency of hypericin compared with chlorin and hematoporphyrin derivatives in HEP-2 and Vero epithelial cell lines, *Photodiagnosis Photodyn. Ther.* 12 (2) (2015) 176–185.
- [51] T. Osmalek, T. Gośliński, J. Mielcarek, E. Osmalek, New trends and safety of photodynamic therapy, *Przegląd Lekarski* 69 (2012) 1205–1208.
- [52] L.A. Muehlmann, G.A. Joanitti, J.R. Silva, J.P.F. Longo, R.B. Azevedo, Liposomal photosensitizers: potential platforms for anticancer photodynamic therapy, *Braz. J. Med. Biol. Res.* 44 (2011) 729–737.
- [53] D. Bechet, P. Couleaud, C. Frochet, M. Viorot, F. Guillemain, M. Berber-Heyob, Nanoparticles as vehicles for delivery of photodynamic therapy agents, *Trends Biotechnol.* 26 (2008) 612–621.
- [54] D.K. Chatterjee, L.S. Fong, Y. Zhang, Nanoparticles in photodynamic therapy: an emerging paradigm, *Adv. Drug Deliv. Rev.* 60 (2008) 1627–1637.
- [55] S. Wang, R. Gao, F. Zhou, M. Selke, Nanomaterials and singlet oxygen photosensitizers: potential applications in photodynamic therapy, *J. Mater. Chem.* 14 (2004) 487–493.
- [56] S. Biswas, V.P. Torchilin, Nanopreparations for organelle-specific delivery in cancer, *Adv. Drug Deliv. Rev.* 66 (2014) 26–41.
- [57] T. Lian, R.J.Y. Ho, Trends and developments in liposome drug delivery systems, *J. Pharm. Sci.* 90 (2001) 667–680.
- [58] V.K. Sharma, D.N. Mishra, A.K. Sharma, B. Srivastava, Liposomes: present prospective and future challenges, *Int. J. Curr. Pharm. Res. Rev.* 1 (2010) 6–16.
- [59] M.M. Amiji, Nanotechnology for Cancer Therapy, CRC Press, New York, 2006.
- [60] A.S.L. Derycke, P.A.M. de Witte, Liposomes for photodynamic therapy, *Adv. Drug Deliv. Rev.* 56 (2004) 17–30.
- [61] D.D. Lasic, D. Papahadjopoulos, Medical Applications of Liposomes, Elsevier, Amsterdam, 1998.
- [62] A. Sharma, U.S. Sharma, Liposomes in drug delivery: progress and limitations, *Int. J. Pharm.* 154 (1997) 123–140.
- [63] K. Stebelska, P. Wyrozumka, M. Grzybek, A. Sikorski, Characterization and medical applications of liposome constructions, *Adv. Clin. Exp. Med.* 2 (2002) 229–242.
- [64] D.K. Martin, Nanobiotechnology of Biomimetic Membranes, Springer, New York, 2007.
- [65] A. Akbarzadeh, R. Rezaei-Sadabady, S. Davaran, S. Woo Joo, N. Zarghami, Y. Hanifehpour, et al., Liposome: classification, preparation, and applications, *Nanoscale Res. Lett.* 8 (2013) 1–9.
- [66] A.B.M. Sipai, Y. Vandana, V.V. Prasanth, Liposomes: an overview, *J. Pharm. Sci. Innov.* 1 (2012) 13–21.
- [67] M. Badran, K. Shalaby, A. Al-Omrani, Influence of the flexible liposomes on the skin deposition of a hydrophilic model drug, carboxyfluorescein: dependency on their composition, *The Scientific World Journal* 2012 (2012) 1–9.
- [68] N. Dragicevic-Curic, S. Gräfe, B. Gitter, S. Winter, A. Fahr, Surface charged temoporfin-loaded flexible vesicles: in vitro skin penetration studies and stability, *Int. J. Pharm.* 384 (2010) 100–108.
- [69] N. Bertrand, J. Wu, X. Xu, N. Kamaly, O.C. Farokhzad, Cancer nanotechnology: the impact of passive and active targeting in the era of modern cancer biology, *Adv. Drug Deliv. Rev.* 66 (2014) 2–25.
- [70] J. Zhong, L.C. Dai, Targeting liposomal nanomedicine to Cancer therapy, *Technol. Cancer Res. Treat.* 11 (2012) 475–481.
- [71] K.P.S. Kumar, D. Bhowmik, L. Deb, The Pharma Innovation 3 (2012), pp. 29–38.
- [72] K. Shashi, K. Satinder, P. Bharat, Recent trends in liposomes used as novel drug delivery system, *Int. Res. J. Pharm.* 3 (2012) 10–16.
- [73] J. Gubernator, Active methods of drug loading into liposomes: recent strategies for stable drug entrapment and increased in vivo activity, *Expert Opin. Drug Deliv.* 8 (2011) 565–580.
- [74] A.S. Ulrich, Biophysical aspects of using liposomes as delivery vehicles, *Biosci. Rep.* 22 (2002) 129–150.
- [75] C. Allen, N. Dos Santos, R. Gallagher, G.N.C. Chiu, Y. Shu, W.M. Li, et al., Controlling the physical behavior and biological performance of liposome formulations through use of surface grafted poly(ethylene glycol), *Biosci. Rep.* 22 (2002) 225–250.
- [76] A. Samad, Y. Sultana, M. Aqil, Liposomal drug delivery systems: an update review, *Curr. Drug Deliv.* 4 (2007) 297–305.
- [77] D.D. Lasic, Novel applications of liposomes, *Trends Biotechnol.* 16 (1998) 307–321.
- [78] K.V. Vousden, X. Lu, Live or let die: the cell's response to p53, *Nat. Rev. Cancer* 2 (2002) 594–604.
- [79] A. Szarkowska, R. Olszewski, J. Zawacka-Pankau, Farmakologiczna aktywacja supresora nowotworu, natywnego białka p53 jako obiecująca strategia zwalczania nowotworów, *Postępy Higieny i Medycyny Doświadczalnej* 64 (2010) 396–407 (in Polish).

- [80] J. Zawacka-Pankau, J. Krachulec, I. Grulkowski, K.P. Bielawski, G. Selivanova, The p53-mediated cytotoxicity of photodynamic therapy of cancer: recent advances, *Toxicol. Appl. Pharmacol.* 232 (2008) 487–497.
- [81] H. Zhao, D. Xing, Q. Chen, New insights of mitochondria reactive oxygen species generation and cell apoptosis induced by low dose photodynamic therapy, *Eur. J. Cancer* 47 (2011) 2750–2761.
- [82] D. Kessel, N.L. Oleinick, Initiation of autophagy by photodynamic therapy, *Methods Enzymol.* 453 (2009) 1–16.
- [83] A.P. Castano, T.N. Demidova, M.R. Hamblin, Mechanisms in photodynamic therapy: part two-cellular signaling, cell metabolism and modes of cell death, *Photodiagnosis Photodyn. Ther.* 2 (2005) 1–23.
- [84] K. Plaetzer, T. Kiesslich, T. Verwanger, B. Krammer, The modes of cell death induced by PDT: an overview, *Med. Laser Appl.* 13 (2003) 7–19.
- [85] E.C. De Bruin, J.P. Medema, Apoptosis and non-apoptotic deaths in cancer development and treatment response, *Cancer Treat. Rev.* 34 (2008) 737–749.
- [86] V.P. Torchilin, Recent advances with liposomes as pharmaceutical carriers, *Nat. Rev. Drug Discov.* 4 (2005) 145–160.
- [87] A.S. Sobolev, D.A. Jans, A.A. Rosenkranz, Targeted intracellular delivery of photosensitizers, *Prog. Biophys. Mol. Biol.* 73 (2000) 51–90.
- [88] C.A. Robertson, E.D. Hawkins, H. Abrahamse, Photodynamic therapy (PDT): a short review on cellular mechanisms and cancer research applications for PDT, *J. Photochem. Photobiol. B* 96 (2009) 1–8.
- [89] M. Sivasankar, T. Katyayan, Liposomes – the future of formulations, *International Journal of Research in Pharmacy and Chemistry* 1 (2) (2011) 259–267.